TABLE OF CONTENTS

	Page	
SUMMARY	1	1/A6
INTRODUCTION	2	1/A7
RELATED WORK	4	1/A9
Secondary Flow Theory	4	1/A9
Forward-Marching Algorithms	4	1/A9
Initial Value Methods	5	1/A10
Global Iteration Methods	7	1/A12
ANALYSIS	9	1/A14
Primary-Secondary Velocity Decomposition	9	1/A14
Surface Potential Equations	10	1/B1
Primary Momentum and Pressure Approximation	11	1/B2
Secondary Vorticity	14	1/B5
Energy Equation	16	1/B7
Compressibility Relations	16	1/B7
Viscous and Heat Conduction Terms	17	1/B8
Governing System of Equations	18	1/B9
Numerical Method	19	1/B10
Summary of Algorithm	19	1/B10
Computed Results	22	1/B13
Laminar Flow Comparisons	22	1/B13
Turbulent Duct Flow Comparison	24	1/C1
SUMMARY AND CONCLUSIONS	27	1/C4
APPENDIX A: GOVERNING EQUATIONS IN ORTHOGONAL COORDINATES	29	1/C6
APPENDIX B: TURBULENCE MODEL	32	1/C9
REFERENCES	36	1/C13
FIGURES	39	1/D2

MAR 1 0 1981

Item 830-H-14

NAS 1.26:3388

ORIGINAL

COMPLETED

NASA Contractor Report 3388

Prediction of Laminar and Turbulent Primary and Secondary Flows in Strongly Curved Ducts

J. P. Kreskovsky, W. R. Briley,
and H. McDonald

CONTRACT NAS3-22014
FEBRUARY 1981

NASA

60

NASA Contractor Report 3388

[illegible]

Prediction of Laminar and Turbulent Primary and Secondary Flows in Strongly Curved Ducts

J. P. Kreskovsky, W. R. Briley,
and H. McDonald
Scientific Research Associates, Inc.
Glastonbury, Connecticut

Prepared for
Lewis Research Center
under Contract NAS3-22014

National Aeronautics
and Space Administration

**Scientific and Technical
Information Branch**

1981

BLANK PAGE

BLANK PAGE

TABLE OF CONTENTS

	Page
SUMMARY	1
INTRODUCTION	2
RELATED WORK	4
Secondary Flow Theory	4
Forward-Marching Algorithms	4
Initial Value Methods	5
Global Iteration Methods	7
ANALYSIS	9
Primary-Secondary Velocity Decomposition	9
Surface Potential Equations	10
Primary Momentum and Pressure Approximation	11
Secondary Vorticity	14
Energy Equation	16
Compressibility Relations	16
Viscous and Heat Conduction Terms	17
Governing System of Equations	18
Numerical Method	19
Summary of Algorithm	19
Computed Results	22
Laminar Flow Comparisons	22
Turbulent Duct Flow Comparison	24
SUMMARY AND CONCLUSIONS	27
APPENDIX A: GOVERNING EQUATIONS IN ORTHOGONAL COORDINATES	29
APPENDIX B: TURBULENCE MODEL	32
REFERENCES	36
FIGURES	39

SUMMARY

Numerical solutions are presented for three-dimensional laminar and turbulent flow in curved ducts of rectangular cross section and significant curvature. The analysis is based on a primary-secondary velocity decomposition in a given coordinate system, and leads to approximate governing equations which correct an *a priori* inviscid solution for viscous effects, secondary flows, total pressure distortion, heat transfer, and internal flow blockage and losses. Solution of the correction equations is accomplished as an initial-value problem in space using an implicit forward-marching technique. The overall solution procedure requires significantly less computational effort than Navier-Stokes algorithms. The present solution procedure is effective even with the extreme local mesh resolution which is necessary to resolve near-wall sublayer regions in turbulent flow calculations. Computed solutions for both laminar and turbulent flow compare very favorably with available analytical and experimental results. The overall method appears very promising as an economical procedure for making detailed predictions of viscous primary and secondary flows in highly curved passages.

INTRODUCTION

An economical method for predicting three-dimensional turbulent subsonic flow in curved flow passages is of considerable value in turbomachinery applications. Of particular interest here is the flow and heat transfer in curved passages including those shaped like the flow passage between adjacent blades of a turbine. In this application, the ultimate goal is the detailed prediction of secondary flows, heat transfer and aerodynamic losses in turbine blade passages. This problem is of particular importance for gas turbine design, since endwall cooling becomes a critical problem as turbine inlet temperatures are increased to achieve high cycle efficiencies. It is generally believed that heat transfer to the turbine endwall and endwall losses are strongly influenced by the large secondary flows which exist in turbine airfoil passages. These secondary flows, which are caused by the turning of the primary flow, can remove insulating endwall boundary layer fluid and replace it with hot mainstream gases, thereby increasing endwall heat transfer. The secondary flows also represent angular momentum not recoverable as thrust and thus are losses which are of prime concern to the turbine designer.

A definitive approach for computation of three-dimensional flow in curved passages would be numerical solution of the Navier-Stokes equations. Although feasible, in three dimensions this approach requires considerable computational effort and is most attractive when no viable alternative exists. The present study considers an alternative approach for predicting such flows and is a development of the primary-secondary velocity decomposition method of Briley and McDonald [1] for application to viscous subsonic flow in smoothly curved geometries. The objective of this approach is to introduce approximations which adequately represent essential physical processes of interest and yet lead to governing equations which can be solved much more economically than the Navier-Stokes equations. In the present treatment of developing flows in curved passages, it is presumed necessary to provide an adequate representation of primary flows, secondary flows, viscous effects, and their local interactions. In the approach taken here, an inviscid flow approximation is first obtained for the geometry in question. The inviscid flow may, for example, satisfy an elliptic governing equation requiring downstream boundary conditions (e.g. a velocity potential equation) and thus include transverse variations in streamwise pressure gradient usually associated with flow in curved passages. This *a priori* inviscid flow is then corrected by solution of a set of approximate governing equations and boundary

conditions which constitute a well-posed initial-value problem in space. These correction equations apply in both viscous and inviscid regions and account for secondary flows, viscous effects, heat transfer, total pressure distortion, and internal-flow blockage and losses. Solution of the correction equations as an initial-value problem provides the desired reduction in computational effort of one or more orders of magnitude over Navier-Stokes solution procedures.

The present development of this approach includes an improved solution algorithm which provides for solution of a pair of correction equations (governing vorticity and vector potential) as a coupled system, using an iterative linearized block implicit (LBI) scheme. This improvement permits implicit specification of no-slip boundary conditions for the secondary flow velocities and removes a previous assumption that flow in the near wall region is collateral. The method is used to compute laminar and turbulent flow in curved ducts of rectangular cross section, and these results are compared with experimental measurements and other numerical predictions.

RELATED WORK

Secondary Flow Theory

The concept of dividing the flow into primary and secondary components is central to the present formulation of an initial-value correction to an a priori inviscid flow approximation. The presence of strong secondary flows is also of particular importance in applications of interest here, and the insight afforded by secondary flow theory is thus of considerable value. Excellent reviews of secondary flow theory and its applications are given by Hawthorne [2,3] and Horlock and Lakshminarayana [4]. A key and relevant feature of many studies based on secondary flow theory is that they provided a basis for treatment of strong rotational but inviscid secondary flows as an initial-value problem, without the necessity of a three-dimensional iteration procedure (cf. Rowe [5]). Previous approaches based on secondary flow theory have generally neglected viscous effects, however, and instead have introduced a somewhat arbitrary "cut off" velocity to exclude the viscous region. Hawthorne [2] has pointed out that ambiguity of the "cut off" velocity can have a significant effect on the predictions obtainable from the inviscid theory. The present approach includes a detailed representation of viscous effects on both primary and secondary flows, and since no distinction between inviscid and viscous flow regions is required, there is no need to introduce a "cut off" velocity. This is accomplished by introducing approximations into a generalized (exact) expression from viscous secondary flow theory given by Lakshminarayana and Horlock [6]. In addition to viscous effects, the present treatment also accounts for generation of secondary vorticity by inviscid mechanisms such as turning of streamlines, for transport of secondary vorticity, and for distortion of the primary flow.

Forward-Marching Algorithms

In recent years, a variety of numerical methods based on forward marching algorithms have been devised for approximating three-dimensional viscous flows for which one "primary" velocity component does not change sign (separate). These methods are often characterized by terminology such as "parabolized Navier-Stokes", "parabolic flow", "partially-parabolic flow", etc., because elements of either the solution procedure or some of the equations solved or both have "parabolic" or "elliptic" qualities. Unfortunately, this terminology does not identify the relevant

physical approximations made or their significance, and does not distinguish these approximations from properties of the solution algorithm and the differential or difference equations. Different methods within the same "category" will in some instances give significantly different results.

Here, methods are identified as either initial-value methods or methods which require three-dimensional iteration, and an attempt is made to identify the most important assumptions made. Although some type of forward-marching algorithm may be used in both the initial value and global iteration approaches, the present distinction is intended to emphasize that initial-value methods provide a solution after a single forward-marching integration and normally require significantly less computational effort than global iteration methods. Global iteration methods on the other hand provide a solution to the system of governing equations only upon convergence of the iterative process. This distinction between the two categories is important, since the approximations made in a proposed method should permit a reduction in computational effort which justifies their use vis-a-vis solving the Navier-Stokes equations without approximation. As a comparison familiar to the present authors, recently developed split linearized block implicit (LBI) algorithms [7] have achieved CDC 7600 run times on the order of 5 minutes per 1000 grid points for the compressible Navier-Stokes equations in three dimensions [8]. The initial-value correction method employed in the present study requires about 20 seconds per 1000 grid points, a 15:1 savings.

Initial Value Methods

Patankar and Spalding [9] and Caretto, Curr, and Spalding [10] formulated equivalent sets of approximate governing equations for use in treating a class of three-dimensional viscous flows without primary flow reversal. They derived these governing equations by neglecting streamwise diffusion and assuming that streamwise pressure gradients are independent of the transverse coordinates. This assumption can be viewed as equivalent to adding a mean correction to pressure gradients from an inviscid flow with constant velocity, and is thus appropriate for flow geometries without significant curvature. In Refs. [9] and [10], numerical methods for treating these equations were proposed. The numerical method of Patankar and Spalding [9] has since been widely used and introduces a further assumption that streamwise increments

in computed transverse pressure gradients are proportional to transverse-velocity corrections introduced to satisfy continuity. The particular pressure-velocity relationship is obtained by neglecting all off-diagonal terms in finite difference formulas which approximate the transverse momentum equations. As a consequence, the computed transverse pressure distribution does not satisfy a (numerically) consistent difference approximation of the transverse momentum equations evaluated with continuity-corrected velocities, except for fully-developed flows for which velocity and pressure corrections are uniformly zero.

As a means of treating flow geometries with significant curvature, Briley [11] suggested an alternative formulation in which streamwise pressure gradients are approximated as the sum of gradients from a potential flow solution in the curved geometry and a mean correction which is independent of transverse coordinates. Here, the assumption is that the potential flow is to be corrected and that the mean pressure drop computed as part of the initial value correction process does not vary across the duct cross-section. In the numerical method of Briley [11], it is assumed that transverse-velocity corrections introduced to satisfy continuity are irrotational; however, the transverse momentum equations are re-solved to obtain the transverse pressure distribution consistent with the continuity-corrected velocities.

Ghia and Sokhey [12] have extended the formulation of Patankar and Spalding [9] and numerical method of Briley [11] to treat incompressible flow in straight or circular arc ducts with either rectangular or polar cross sections. They were successful in obtaining solutions for laminar flow development in circular arc ducts of rectangular cross section and strong curvature.

As part of a comprehensive study of developing flow in straight rectangular ducts, Rubin and Khosla [13] derived from asymptotic theory a system of governing equations based on velocity, vorticity, and a potential and stream function for the crossflow. These equations are valid in the "fully viscous" region also addressed by the initial-value methods of [9-12]. The Rubin-Khosla governing equations are independent of Reynolds number, and are solved numerically as an initial value problem without further approximation.

The present study is a development of the initial-value correction approach of Briley and McDonald [1] and provides a general method for treating flows in smoothly curved geometries which may have significant streamwise curvature and turning. This method is based on a primary-secondary velocity decomposition in a given coordinate system. Unlike most previous methods, the primary flow velocity component may or may not be aligned with the marching coordinate direction. The primary flow is governed

by a momentum equation in which streamwise pressure gradients are approximated from an a priori inviscid-flow analysis, computation, or approximation. The secondary flow is uniquely determined, through scalar and vector surface potential calculations, from the primary velocity and secondary or streamwise vorticity, the latter of which is computed here from an approximation to an exact equation governing viscous secondary flows. This system of equations corrects an a priori inviscid solution for viscous effects, secondary flows, total pressure distortion, heat transfer and internal flow blockage. Solution of the correction equations is accomplished as an initial-value spatial marching process. The dependent variables (primary velocity, secondary vorticity, scalar and vector surface potentials) are analogous to those used by Rubin and Khosla [13] in Cartesian coordinates.

Other developments of this particular initial value correction method have been applied to other problems. Shamroth and Briley [14] have obtained predictions for the airfoil tip vortex generation process. Kreskovsky, Briley and McDonald [15] have obtained predictions for turbofan exhaust lobe mixer flows, which requires treatment of turbulent mixing in the curved interface of two flow streams having large differences in stagnation temperature and flow angle, and slight differences in stagnation pressure. Further results for this problem have been computed by Anderson, Povinelli, and Gerstenmaier [16]. The analysis has been reformulated for use with constructed coordinate systems by Levy, McDonald, Briley, and Kreskovsky [17] and applied to duct and diffuser geometries having curved centerlines and superelliptic cross sections.

Global Iteration Methods

Methods within this category neglect streamwise diffusion and employ forward-marching algorithms as part of a global iteration process. Although streamwise diffusion is neglected, the system of governing equations being solved remains elliptic (for subsonic flow) and is thus subject to one or more downstream boundary conditions. To permit the use of forward-marching algorithms under these circumstances, an imbalance is introduced in the system of governing equations during the forward-marching process, either in continuity or in the representation of pressure gradients. Corrections are introduced after each iteration to reduce this imbalance, and the system of equations and boundary conditions is satisfied once the global iteration converges.

The "partially parabolic" method of Pratap and Spalding [18] is a global iteration which begins with a "guessed" pressure field and performs iterated forward marching sweeps of the flow field. During these forward-marching iterations, the three momentum equations are solved for velocity, and two-dimensional velocity and pressure corrections are determined to remove a local imbalance in continuity. Various strategies are then employed to modify the three-dimensional pressure field, so as to improve the local continuity balance on subsequent iterations. Moore and Moore [19] have proposed a somewhat related global iteration method which, given an estimated pressure distribution, computes velocities and a local two-dimensional pressure correction by a forward-marching algorithm. After each forward marching iteration, a three-dimensional global pressure correction is computed from this local two-dimensional pressure correction for use in the next iteration. To provide improved understanding of the predictions and possibly increase the rate of convergence, Moore and Moore [19] suggest converging the global iteration in three separate stages, each of which is itself a global iteration. The complexity of the flow model is increased in each stage; first is inviscid flow with uniform inflow, second is inviscid flow with nonuniform stagnation pressure at inflow, and third is viscous flow. Upon convergence such that all pressure and velocity corrections are uniformly zero, it appears that the only assumptions made by the global iteration methods of Pratap and Spalding [18] and Moore and Moore [19] are the neglect of streamwise diffusion, the condition of no reversed flow, and approximations introduced through boundary conditions and turbulence modeling.

Dodge [20] has suggested a global iteration method which divides the velocity vector into rotational and irrotational portions which become defined only upon convergence of the global iteration and upon selection of a set of boundary conditions governing the rotational-irrotational velocity division. A key assumption in Dodge's method is that all pressure gradients depend solely on the irrotational component of the velocity vector and are independent of the remaining rotational component. In view of this assumption, the method of Dodge does not seem suitable for applications having regions of rotational but inviscid secondary flow. Dwoyer [21] has also pointed out that the boundary conditions defining the velocity division are arbitrary and has shown that selection of these boundary conditions is crucial.

ANALYSIS

The governing equations are derived through approximations made relative to a curvilinear but not necessarily orthogonal coordinate system fitted to and aligned with the flow geometry under consideration (cf. Fig. 1). The coordinate system is chosen such that the streamwise or marching coordinate either coincides with or is at least approximately aligned with a known inviscid primary flow direction, as determined for example by a potential flow for the given geometry. Transverse coordinate surfaces must be either perpendicular or nearly perpendicular to solid walls or bounding surfaces, since diffusion is permitted only in these transverse coordinate surfaces.

Equations governing a scalar viscous correction u_v to a known inviscid primary flow velocity $\bar{U}_I$, and a secondary vorticity Ω, normal to transverse coordinate surfaces are derived utilizing approximations which permit solution of the correction equations as an initial-value problem, provided reversal of the composite streamwise velocity does not occur. Terms representing diffusion normal to transverse coordinate surfaces are neglected. Approximate pressure gradients are derived from the inviscid primary flow and imposed in the streamwise momentum equation. These pressure gradients are the sole means of accounting for the elliptic influence of downstream boundary conditions in curved flow geometries. The secondary vorticity is computed as an approximate application of viscous secondary flow theory. Secondary flow velocities are determined from scalar and vector surface potential calculations in transverse coordinate surfaces, once the primary velocity and secondary vorticity are known.

Primary-Secondary Velocity Decomposition

In what follows, vectors are denoted by an overbar, and unit vectors by a caret. The analysis is based on decomposition of the overall velocity vector field $\bar{U}$ into a primary flow velocity $\bar{U}_p$ and a secondary flow velocity $\bar{U}_s$. The overall or composite velocity is determined from the superposition

$$\bar{U} = \bar{U}_p + \bar{U}_s \tag{1}$$

The primary flow velocity is represented as

$$\bar{U}_p = \bar{U}_I u_v \tag{2}$$

where $\bar{U}_I$ is a known inviscid primary flow velocity satisfying slip conditions and determined for example from an a priori potential flow solution in the geometry under consideration. The (non-dimensional) scalar quantity u_v is a viscous velocity profile factor which introduces viscous shear layers and may also correct for internal flow blockage effects. The viscous velocity correction u_v is determined from solution of a primary flow momentum equation. The secondary flow velocity $\bar{U}_s$ is derived from scalar and vector surface potentials denoted ϕ and ψ, respectively. If $\hat{i}_1$ denotes the unit vector normal to transverse coordinate surfaces (also presumed here to be in the direction of the marching coordinate), if ρ is density, and if ρ_o is an arbitrary constant reference density, then $\bar{U}_s$ is defined by

$$\bar{U}_s \equiv \nabla_s \phi + (\rho_o/\rho) \nabla \times \hat{i}_1 \psi \tag{3}$$

where ∇_s is the surface gradient operator defined by

$$\nabla_s \equiv \nabla - \hat{i}_1 (\hat{i}_1 \cdot \nabla) \tag{4}$$

It follows that $\hat{i}_1 \cdot \bar{U}_s$ lies entirely within transverse coordinate surfaces. Equation (3) is a general form permitting both rotational and irrotational secondary flows and will lead to governing equations which may be solved as an initial-boundary value problem. The overall velocity decomposition (1) can be written

$$\bar{U} = \bar{U}_I u_v + \nabla_s \phi + (\rho_o/\rho) \nabla \times \hat{i}_1 \psi \tag{5}$$

Surface Potential Equations

Equations relating ϕ and ψ with u_v, ρ, and the secondary vorticity component Ω_1 can be derived using Eq. (5) as follows: From continuity,

$$\nabla \cdot \rho \bar{U} = 0 = \nabla \cdot \rho \bar{U}_I u_v + \nabla \cdot \rho \nabla_s \phi + \rho_o \nabla \cdot \nabla \times \hat{i}_1 \psi \tag{6}$$

and from the definition of the secondary vorticity, Ω_1

$$\hat{i}_1 \cdot \nabla \times \bar{U} \equiv \Omega_1 = \hat{i}_1 \cdot \nabla \times \bar{U}_I u_v + \hat{i} \cdot \nabla \times (\rho_o/\rho) \nabla \times \hat{i}_1 \psi + \hat{i}_1 \cdot \nabla \times \nabla_s \phi \tag{7}$$

Since the last term in each of Eqs. (6,7) is zero by vector identity, Eqs. (6,7) can be written as

$$\nabla \cdot \rho \nabla_s \phi = - \nabla \cdot \rho \bar{U}_I u_v \tag{8}$$

$$\hat{i}_1 \cdot \nabla \times (\rho_o/\rho) \nabla \times \hat{i}_1 \psi = \Omega_1 - \hat{i}_1 \cdot \nabla \times \bar{U}_I u_v \tag{9}$$

The last term in Eq. (9) is identically zero in a coordinate system for which $\hat{i}_1$ and $\bar{U}_I$ have the same direction, and is small if $\hat{i}_1$ and $\bar{U}_I$ are approximately aligned. Further simplification is possible if $\bar{U}_I$ is an incompressible potential flow satisfying $\nabla \cdot \bar{U}_I = \nabla \times \bar{U}_I = 0$, since the last term in each of Eqs. (8) and (9) can then be written $- \bar{U}_I \cdot \nabla \rho u_v$ and $- \hat{i}_1 \cdot \bar{U}_I \times \nabla u_v$, respectively. In any event, given a knowledge of u_v, Ω, and ρ, the surface potentials ϕ and ψ can be determined by a two-dimensional elliptic calculation in transverse coordinate surfaces at each streamwise location. In turn, $\bar{U}_s$ can be computed from Eq. (3), and the composite velocity $\bar{U}$ will satisfy continuity. Equations for u_v and Ω_1 are obtained from the equations governing momentum and vorticity, respectively.

Primary Momentum and Pressure Approximation

The streamwise momentum equation is given by

$$\hat{i}_1 \cdot \left[(\bar{U} \cdot \nabla) \bar{U} + (\nabla p)/\rho \right] = \hat{i}_1 \cdot \bar{F} \tag{10}$$

where p is pressure and $\rho \bar{F}$ is force due to viscous stress. Terms in $\bar{F}$ representing streamwise diffusion are neglected; however, since the viscous terms are complex for compressible flow, the modified viscous force is temporarily denoted $\bar{F}'$, and further consideration of viscous terms is deferred to a later section.

The remaining assumption for Eq. (10) concerns the pressure gradient term and is designed to permit numerical solution as an initial value problem. The assumption that the streamwise pressure gradient is independent of transverse coordinates is inadequate for curved flow geometries, and instead the streamwise pressure gradients are approximated from an inviscid flow obtained by an a priori analysis, computation, or approximation, and are corrected for viscous effects by a mean pressure gradient term which depends only on the x_1 coordinate. An obvious choice for an inviscid velocity $\bar{U}_I$ is the potential flow for the geometry under consideration, although other choices for $\bar{U}_I$ may be used. The inviscid flow may satisfy an elliptic governing equation requiring downstream boundary conditions (e.g. a velocity potential equation) and thus include transverse variations in streamwise pressure gradient usually associated with flow in curved passages.

It is possible to consider the use of pressure gradients from a rotational inviscid flow determined by solution of the Euler equations. It should be pointed out, however, that unlike the scalar potential equation, the computational labor of solving the Euler equations is commensurate with that required for solution of the full Navier-Stokes equations with a similar number of mesh points. Solution of the Euler equations may require fewer grid points since thin shear layers are omitted and hence do not require resolution by the grid used. On the other hand, omitting the shear layers entails further approximation in selecting a "cut-off" criterion between inviscid and viscous regions at inflow (cf. Hawthorne [2]), and the predicted flow may be sensitive to the criterion chosen. Consequently, in pursuing the goal of developing a computationally efficient alternative to solution of the Navier-Stokes equations, the potential flow for the geometry in question is presently being used as the basic flow to be corrected. Methods for improving or correcting the pressure gradients are deferred for a subsequent investigation.

The implications of this type of pressure approximation may be clarified by examination of the inviscid momentum equation written as

$$\nabla p + \rho \nabla (q^2/2) = \rho \bar{U} \times \bar{\Omega} \tag{11}$$

where $q^2 = \bar{U} \cdot \bar{U}$, and vorticity $\bar{\Omega} = \nabla \times \bar{U}$. In an orthogonal coordinate system, the $\hat{i}_1$ component of Eq. (11) is

$$\hat{i}_1 \cdot \left[\nabla p + \rho \nabla (q^2/2) \right] = \rho (u_2 \Omega_3 - u_3 \Omega_2) \tag{12}$$

for small transverse vorticity Ω_2, Ω_3 and small transverse velocities u_2, u_3 (relative to the coordinate system being used), the right-hand side of Eq. (12) is of second order and may be neglected. This "small shear" assumption is familiar as part of the "secondary flow approximation" (cf. Hawthorne [3]), although it should be emphasized that the present analysis accounts for "distortion of Bernoulli surfaces" by means of u_v.

If the right side of Eq. (12) is neglected, if pressure gradients are derived from the inviscid velocity $\bar{U}_I$ by setting $q^2 = \bar{U}_I \cdot \bar{U}_I$, and if a mean viscous pressure correction $p_v(x_1)$ is introduced, the pressure approximation can be written as

$$\hat{i}_1 \cdot \nabla p \doteq \hat{i}_1 \cdot \left[\nabla p_v(x_1) - \rho \nabla (\bar{U}_I \cdot \bar{U}_I)/2 \right] \equiv \hat{i}_1 \cdot \nabla (p_I + p_v) \tag{13}$$

where p_I is the imposed pressure. Typically, for internal flows, p_v is determined to ensure that an integral mass flux condition is satisfied, such as

$$\int_A \hat{i}_1 \cdot \rho \bar{U} \, dA = \text{constant} \tag{14}$$

For external flows, $p_v = 0$. Arguments favoring this pressure approximation lose some validity in strongly curved corner regions, where strong crossflows in the inviscid outer region of shear layers are deflected. Nevertheless, the approximation may not be seriously in error when considering its overall and somewhat limited role in the present context. Finally, this type of pressure approximation is questionable for strongly deflected <u>inviscid</u> flows having large transverse vorticity.

Combining Eqs. (10) and (13) and setting $\bar{F} \doteq \bar{F}'$ provides an equation nominally governing u_v:

$$\hat{i}_1 \cdot \left[(\bar{U} \cdot \nabla)\bar{U} + (\nabla p_v)/\rho - \nabla (\bar{U}_I \cdot \bar{U}_I)/2 \right] = \hat{i}_1 \cdot \bar{F}' \tag{15}$$

where $\bar{U}$ is to be written as

$$\bar{U} = \hat{i}_1 u_I u_v + \hat{i}_2 (v_I u_v + v_s) + \hat{i}_3 (w_I u_v + w_s) \tag{16}$$

where u_I, v_I, w_I are components of $\bar{U}_I$, and v_s, w_s are components of $\bar{U}_s$.

Secondary Vorticity

An equation governing Ω_1 in compressible flow can be obtained from an approximate application of secondary flow theory. The equation governing the growth of vorticity Ω_s along a streamline for incompressible flow with constant viscosity is given by Lakshminarayana and Horlock [6] and may be written as

$$\frac{\partial}{\partial s}\left(\frac{\Omega_s}{\rho q}\right) = \frac{2\Omega_n}{\rho q R} - \frac{1}{\rho q^2}\,\hat{s}\cdot\nabla\times\frac{1}{\rho}\nabla p + \frac{1}{\rho q^2}\,\hat{s}\cdot\bar{G} \tag{17}$$

where q is velocity magnitude, $\hat{s}$ is distance along a streamline, Ω_n is vorticity in the direction of the unit principal normal vector $\hat{n}$ of the streamline, for which R is the principal radius of curvature. These quantities are related by the Frenet formula $\hat{n}/R = \partial s/\hat{s}\cdot\nabla\hat{s}$. In Eq. (17), $\bar{G} \equiv \nabla \times \bar{F}$, and the term containing p vanishes if ρ is constant. Since an intrinsic coordinate system formulation as in Eq. (17) provides an "inverse" coordinate system if used to compute $\bar{U}$, and since intrinsic coordinates are degenerate on no-slip surfaces and nonorthogonal for general rotational flows, intrinsic coordinates are not attractive for numerical computation. However, if the coordinate system used for computation is approximately aligned with the flow direction, then an approximate equation governing Ω_1 can be derived from Eq. (17) by replacing $\hat{s}$ by $\hat{i}$, as in the following development:

$$\frac{\Omega_s}{q} = \frac{\hat{s}\cdot\bar{\Omega}}{\hat{s}\cdot\bar{U}} \doteq \frac{\hat{i}_1\cdot\bar{\Omega}}{\hat{i}_1\cdot\bar{U}} = \frac{\Omega_1}{u_1} \tag{18a}$$

$$\frac{\Omega_n}{qR} = \frac{(\hat{s}\cdot\nabla\hat{s})\cdot\bar{\Omega}}{\hat{s}\cdot\bar{U}} \doteq \frac{(\hat{i}_1\cdot\nabla\hat{i}_1)\cdot\bar{\Omega}}{\hat{i}_1\cdot\bar{U}} = \frac{\Omega_{n1}}{u_1 R_1} \tag{18b}$$

where $u_1 = u_1 u_v$; R_1 is the principal radius of curvature of the x_1 coordinate, and Ω_{n1} is vorticity in the direction of $\hat{n}_1$, the principal normal of the x_1 coordinate line. The quantities $\hat{n}_1$ and R_1 are defined by the Frenet formula $\hat{n}_1/R_1 = \hat{i}_1\cdot\nabla\hat{i}_1$. To illustrate, in an orthogonal coordinate system,

$$\frac{\hat{n}_1}{R_1} = -\left[\frac{\hat{i}_2}{h_1 h_2}\frac{\partial h_1}{\partial x_2} + \frac{\hat{i}_3}{h_1 h_3}\frac{\partial h_1}{\partial x_3}\right] \tag{19}$$

where h_1, h_2, h_3 denote metric coefficients. If ρ varies, p is replaced by the imposed pressure p_I as defined in Eq. (13). Finally, taking $q^2 \doteq u_1^2$ and $\hat{s} \doteq \hat{i}_1$ in the last two terms in Eq. (17), and neglecting streamwise diffusion, Eq. (17) becomes

$$\bar{U}\cdot\nabla\left(\frac{\Omega_1}{\rho u_1}\right) = \frac{2\Omega_{n1}}{\rho u_1 R_1} - \frac{1}{\rho u_1^2}\hat{i}_1\cdot\nabla\times\left(\frac{\nabla p_I}{\rho}\right) + \frac{1}{\rho u_1^2}\hat{i}_1\cdot\bar{G}' \qquad (20)$$

where $\bar{G}'$ does not contain streamwise diffusion.

The transverse vorticity Ω_{n1} in Eq. (20) contains components which, in orthogonal coordinates and assuming an irrotational $\bar{U}_I$, are given by

$$\Omega_2 = \hat{i}_2\cdot\nabla\times\bar{U} = \frac{u_I}{h_3}\frac{\partial u_v}{\partial x_3} - \frac{w_I}{h_1}\frac{\partial u_v}{\partial x_1} - \frac{1}{h_1 h_3}\frac{\partial}{\partial x_1}(h_3 w_s) \qquad (21a)$$

$$\Omega_3 = \hat{i}_3\cdot\nabla\times\bar{U} = -\frac{u_I}{h_2}\frac{\partial u_v}{\partial x_2} + \frac{v_I}{h_1}\frac{\partial u_v}{\partial x_1} + \frac{1}{h_1 h_2}\frac{\partial}{\partial x_1}(h_s v_s) \qquad (21b)$$

In the applications contemplated here, the first term on the right-hand side of each of Eqs. (21a-b) is expected to dominate, and the remaining terms may be neglected as a convenience, if desired.

An alternative equation governing vorticity can be derived from the general vector equation for vorticity in compressible flow:

$$(\bar{U}\cdot\nabla)\bar{\Omega} - (\bar{\Omega}\cdot\nabla)\bar{U} + \bar{\Omega}(\nabla\cdot\bar{U}) + \nabla\times\frac{1}{\rho}\nabla p = \bar{G} \qquad (22)$$

Streamwise diffusion is neglected in Eq. (22), and if ρ varies, p is replaced by p_I. Utilizing continuity and relationships valid for general orthogonal coordinates, the x_1 component of Eq. (22) can be written as

$$\bar{U}\cdot\nabla\Omega_1 - \bar{\Omega}\cdot\nabla u_1 + (\Omega_1\bar{U} - u_1\bar{\Omega})\cdot\frac{\hat{n}_1}{R_1} - \frac{\Omega_1}{\rho}\bar{U}\cdot\nabla\rho + \hat{i}_1\cdot\nabla\times\frac{1}{\rho}\nabla p_I = \hat{i}\cdot\bar{G}' \qquad (23)$$

The last two terms on the left side of Eq. (23) vanish if ρ is constant. Because of insight provided by previous work on secondary flow theory, Eq. (20) was used instead of Eq. (23) in the present application to curved flow geometries.

Energy Equation

If the flow being considered is nonadiabatic, solution of an equation governing energy is required. The energy equation can be written in a variety of forms, one of which is

$$\rho\bar{U}\cdot\nabla E = \nabla\cdot k\nabla T + \bar{U}\cdot\bar{F} + \Phi \tag{24}$$

where E is total enthalpy, T is temperature, k is thermal conductivity, and Φ is the dissipation function. Solution of Eq. (24) by forward marching integration requires only that terms representing streamwise conduction of heat and also streamwise viscous diffusion in $\bar{F}$ be neglected.

Compressibility Relations

The foregoing analysis can be applied to incompressible flows simply by setting $\rho \equiv \rho_o$. Compressibility effects are represented by introducing the perfect gas equation of state $p = \rho RT$ in the imposition of streamwise pressure gradients. For moderate subsonic Mach numbers, inviscid pressure gradients can be obtained either from a compressible potential flow calculation or from an incompressible potential flow corrected for compressibility using either the Prandtl-Glauert formula, Laitone's variant [22], or the recent suggestion of Lieblein and Stockman [23]. Replacing ρ in Eq. (13) by the state equation and eliminating temperature using the temperature-enthalpy relation

$$E = c_p T + \frac{\bar{U}\cdot\bar{U}}{2} \tag{25}$$

where c_p denotes specific heat, the following auxiliary equation relating the imposed pressure gradients with density, velocity,and total enthalpy is obtained:

$$\hat{i}_1\cdot\nabla\left[p_I + p_v(x_1)\right] = \hat{i}_1\cdot\nabla\left[\frac{\gamma-1}{\gamma}\rho\left(E - \frac{\bar{U}\cdot\bar{U}}{2}\right)\right] \tag{26}$$

where γ is specific heat ratio. A slight simplification results if $\bar{U}\cdot\bar{U}$ is replaced by $(\hat{i}_1\cdot\bar{U})^2$ in Eq. (26).

In many problems of interest, it can be assumed that the total enthalpy is a constant E_o. This assumption is reasonable for inviscid flow regions with no heat addition and for boundary layers on adiabatic walls provided the Prandtl number is unity. To make this assumption, E is replaced by E_o in Eq. (26), and it is then unnecessary to solve the energy equation, even though the flow is compressible.

Typically, the treatment of nonconstant total enthalpy is of interest for predicting heat transfer levels in wall boundary layers. However, it should be noted that the geometrical pattern of streamlines for steady inviscid flow of a perfect gas depends only on the total pressure gradient and not on the distribution of total enthalpy (cf. Hawthorne [3]). Thus, within an assumption of small transverse total pressure gradient in the free stream or core region, it is possible to consider core flows with two separate streams having large differences in total enthalpy and velocity and hence separated by thermal and viscous shear layers, provided the two streams have about the same static and total pressure. This observation was used to advantage by Kreskovsky, Briley and McDonald [15] in an application of the present analysis to flow in turbofan exhaust lobe mixers.

Viscous and Heat Conduction Terms

A variety of techniques for suppressing streamwise diffusion is possible, and the particular choice in any given application may depend on the complexity one is willing to tolerate in the viscous terms. For example, the complete set of viscous terms can be written out and all derivatives in the streamwise direction neglected. Alternatively, only second derivatives in the streamwise direction may be neglected. Here, attention is restricted to incompressible flow but with variable viscosity. In the momentum equation (10), $\bar{F} \equiv -\nabla \times \nu \nabla \times \bar{U}$, where ν is kinematic viscosity. A particularly simple expression which neglects contributions from $\bar{U}_s$ is given by

$$\hat{i}_l \cdot \bar{F} \triangleq -\hat{i}_l \cdot \nabla \times \nu \nabla \times \hat{i}_l u_I u_v = \bar{F}' \tag{27}$$

Alternatively, contributions from $\bar{U}_s$ may be retained as in the approximation

$$\hat{i}_l \cdot \bar{F} \triangleq -\hat{i}_l \cdot \nabla \times \nu \nabla_s \times \bar{U} = \bar{F}' \tag{28}$$

Similarly, in the vorticity equation (17), $\bar{G}$ is defined by $\bar{G} = -\nabla \times \nabla \times \nu\bar{\Omega}$ and approximated by

$$\hat{i}_l \cdot \bar{G} \doteq -\hat{i}_l \cdot \nabla \times \nabla \times \hat{i}_l \nu \Omega_l \equiv \bar{G}' \tag{29}$$

Streamwise heat conduction in Eq. (24) is suppressed by the approximation

$$\nabla \cdot k \nabla T \doteq \nabla \cdot k \nabla_s T \tag{30}$$

Governing System of Equations

A complete system of six coupled equations governing u_v, Ω_l, ϕ, ψ, E, and ρ is given by Eqs. (8), (9), (15), (24), (26), and (20) or (23). Ancillary relations are given by Eq. (5) for composite velocity, Eq. (14) for mass flux, and Eqs. (21a-b) for transverse vorticity, Eq. (26) may be omitted if ρ is constant, and Eq. (24) may be omitted for constant E. In the Appendix, these equations are given in general orthogonal coordinates.

Numerical Method

Since techniques for obtaining the basic potential flow solution are well known and numerous, they need not be enumerated or discussed here. Instead, the present development concentrates on describing the numerical method used to solve the system of correction equations. Streamwise derivative terms in the governing equations have a form such as $u_1 \partial( )/\partial x_1$, and because the streamwise velocity u_1 is very small in the viscous dominated region near no-slip walls, it is essential to use implicit algorithms which are not subject to stringent stability restrictions unrelated to accuracy requirements. Although it is possible to devise algorithms for solution of the correction equations as a fully coupled implicit system, such algorithms would require considerable iteration for the system of equations treated here, and this would detract from the overall efficiency. The present method is semi-implicit and seeks to reduce the amount of iteration required and yet avoid the more severe stability restrictions of explicit algorithms. The method partitions the system of correction equations into subsystems which govern the primary flow, the secondary flow, and the turbulence model. The primary-flow subset of equations contains the streamwise momentum and energy equations, the state equation, and the integral mass flux relation. The secondary-flow subset of equations contains the secondary vorticity equation and the scalar and vector potential equations. The turbulence model in the present study includes a turbulence kinetic energy equation and a length scale relationship. These subsystems are decoupled using an ad hoc linearization in which secondary velocity components and turbulent viscosity are lagged, and are solved sequentially during each axial step.

Summary of Algorithm

The correction equations are replaced by finite-difference approximations. Three-point central difference formulas are used for all transverse spatial derivatives. An analytical coordinate transformation devised by Roberts [24] is employed as a means of introducing a nonuniform grid in each transverse coordinate direction, as appropriate, to concentrate grid points in the wall boundary layer regions. Second-order accuracy for the transverse directions is rigorously maintained. Two-point backward difference approximations are used for streamwise derivatives, although this is not essential.

To solve the primary flow subsystem of viscous correction equations, scalar ADI schemes are used for the momentum and energy equations, and the standard secant iteration process [25] is used to find the mean pressure drop consistent with the integral mass flux relationship and state equation. It is convenient to choose $u_1 \equiv u_I\ u_v$ as the dependent variable for the primary flow momentum equation.

Given the solution for the primary flow, the secondary flow subsystem can be solved. First the scalar potential equation (continuity) is solved using a scalar iterative ADI scheme. Next, the secondary vorticity and vector potential equations are written as a fully implicit coupled system and solved using an iterative linearized block implicit (LBI) scheme (cf. Briley and McDonald [7]). In selecting boundary conditions for the secondary flow subsystem, care must be taken to ensure that the final secondary velocity satisfies the no-slip condition accurately. Zero normal derivatives of ϕ are specified in the scalar potential equation, and this boundary condition corresponds to zero normal velocity. It is not possible to simultaneously specify the tangential velocity, however, and thus the ϕ-contribution to the secondary velocity will have a nonzero tangential (slip) component, denoted v_t, at solid boundaries. In the coupled vorticity-vector-potential equations, both normal and tangential velocity components can be specified as boundary conditions, since these equations are solved as a coupled system. By choosing (a) zero normal velocity and (b) $-v_t$ as the ψ-contribution to the tangential velocity, the slip velocity v_t arising from the ϕ calculation is cancelled, and the composite secondary flow velocity including both ϕ and ψ contributions will satisfy the no-slip condition exactly.

Finally, the turbulence model requires solution of the turbulence kinetic energy equation, and this is done using a scalar ADI scheme.

A summary of the overall algorithm used to advance the solution a single axial step follows. It is assumed that the solution is known at the n level x^n and is desired at x^{n+1}.

(1) The imposed streamwise pressure gradient distribution is determined from an *a priori* inviscid potential flow.

(2) A value for the mean viscous pressure drop p_v^{n+1} is assumed. Initially, the value from the previous step p_v^n is used.

(3) The momentum equation is solved to determine u_1^{n+1}, and if this is the first secant iteration for the mean pressure drop, the energy equation is also solved for E^{n+1}.

(4) The density is determined from the equation of state, using the imposed pressure with mean correction added, and using u_1^{n+1} and E^{n+1}.

(5) Since for internal flows, the integral mass flux relation (14) will generally not be satisfied, return to step (2) and repeat this process iteratively using the standard secant method [25] to find the value of p_v^{n+1} which leads to u_1^{n+1} and ρ^{n+1} satisfying the integral mass flux relation (14). The secant method was found in practice to converge to five figures on the third iteration.

(6) Using values now available for ρ^{n+1} and u_1^{n+1}, the scalar potential equation (8) is solved using an iterative scalar ADI scheme, to obtain ϕ^{n+1}. This ensures that the continuity equation is satisfied.

(7) The equations for vorticity (20) and vector potential (9) form a coupled system for Ω_1^{n+1} and ψ^{n+1} which is solved as a coupled system using an iterative LBI scheme.

(8) Values for the transverse velocities v_s and w_s are computed from Eq. (3).

(9) The turbulence kinetic energy equation is solved using a scalar ADI scheme. Updated values of μ_t are then computed from k^{n+1} and the specified length scale. The turbulence model used here is given in the Appendix.

Computed Results

Three solutions have been computed for flow in rectangular ducts with significant curvature, to assess the present analysis and computational method. The first case is a laminar flow with thin boundary layers and is compared with analytical and experimental results. The second case is a laminar flow which becomes fully developed and is compared with an analytical solution for fully developed flow. The third case is a turbulent flow in the curved section of a 90° bend with straight extensions at the inlet and exit. This flow has moderate boundary layer thickness, and detailed comparisons of primary and secondary velocity profiles with available experimental measurements are made.

Laminar Flow Comparisons

Horlock, Lewkowicz and Wordsworth [26] have measured the yaw angle profile in a three-dimensional laminar boundary layer on the endwall of a circular arc duct with a free stream which approximates a free vortex flow ($u_I r$ = constant). The duct has a curvature ratio R/H = 3.5, where R is the centerline radius of curvature defined as the average of ineer and outer duct radii, $R = (R_i + R_o)/2$, and H is the radial duct width, $H = R_o - R_i$. The Reynolds number Re_H of the experimental flow is 250,000. The Horlock-Wordsworth [27] similarity theory shows that for such a free-vortex flow the boundary layer yaw angle profile in Blasius coordinates is independent of Reynolds number, and thus the present calculation was performed for Re_H = 10,000 to produce a thicker boundary layer requiring fewer grid points for adequate resolution. In addition, to avoid the leading edge singularity, the calculation was initiated at a distance 0.04H downstream of the leading edge of the test surface, and streamwise velocity profiles matching the Blasius boundary layer thickness δ = 0.01 H were specified at this location. As part of the starting procedure, a secondary flow velocity distribution was constructed to account for secondary vorticity generated by turning of the flow through the angle of 0.6° from the leading edge to 0.04H. This was estimated from the Squire-Winter [28] secondary flow theory and corrected in the viscous region for no-slip conditions. A further correction was made to satisfy the continuity equation at the starting location. A 20 x 20 locally refined mesh was used for the transverse coordinate surface, and 19 streamwise stations were computed using a geometrically increasing step size ($\Delta x_{i+1}/\Delta x_i$ = 1.05). This required about 2.5 minutes of CDC 7600 run time.

The computed and measured yaw angle profiles are compared in Fig. 2, and the agreement is generally good except near the outer edge of the boundary layer, where Horlock, et al expressed concern that residual swirl may have affected their measurements. The present calculation also includes the region of very strong skewing near the endwall surface, and predicts a maximum yaw angle of about 26 degrees on the wall. This compares with a free stream angle of turning of only 12 degrees. The present results are also in good agreement with the Horlock-Wordsworth similarity solution, as evaluated by Horlock, et al [25] using the experimentally measured pressure distribution. The present calculations employed pressure gradients from the free vortex potential flow ($u_I r$=constant), and these are corrected for mean pressure drop.

Further results from the present computed solution are shown in Figs. 3-5. In Fig. 3, contours of streamwise velocity and a vector plot of the secondary flow are shown for the cross-sectional plane at the experimental measuring station. Although the present results have a boundary layer thickness five times larger than Horlock's experiment (due to the differing Reynolds numbers), it is evident from Fig. 3 that the present case does represent a thin boundary layer flow in the center of the duct. A vortex behavior in the suction-surface-endwall corner is also visible in Fig. 3. In Fig. 4, a vector plot of computed velocities in a plane parallel to and one grid point away from the endwall is shown. Here, the gradual development with streamwise distance of skewing or overturning near the endwall (flow deflected toward the inner or suction surface) is evident. In Fig. 5, similar vector plots are shown for the surfaces located one grid point away from inner and outer duct sidewalls ("unwrapped" to lie in a plane). As expected, the flow is deflected toward the endwall near the outer (pressure) surface and away from the endwall near the inner (suction) surface. In summary, the results in Figs. 2-5 from this test calculation tend to confirm the ability of the analysis and solution algorithm to predict laminar developing flow in curved ducts with thin boundary layers.

The second test case consists of laminar flow in a circular arc duct of square cross section under conditions of lower Reynolds number and smaller duct curvature, such that shear layers are thick and eventually fill the duct. This case has R/H = 14, Re_H = 205, Dean number K = 55, defined by $K = Re_H(H/R)^{1/2}$, and inlet Mach number M = 0.01. The inviscid flow was assumed to have $u_I r$ = constant, and inlet boundary layers of thickness 0.1H were prescribed as the starting condition. This calculation was performed on a 20 x 20 nonuniform mesh for the cross section and reached a condition of fully developed flow after about 100 degrees of turning which required 16

axial steps. In Fig. 6, computed results for a typical fully developed radial velocity profile are compared with the calculated results of Ghia and Sokhey [12], which were made under slightly different similarity assumptions for fully developed flow. For fully developed flow, the only difference in the theories are found in the equations governing the secondary flows. The present analysis utilizes a streamwise vorticity equation derived from viscous secondary flow theory, whereas the secondary flow in the results of Ghia and Sokhey is governed by components of the momentum equation in the directions of a polar-cylindrical coordinate system. Nevertheless, Fig. 6 shows that the two predictions are in reasonable agreement. It should be recalled that the present analysis permits optional use of the streamwise component of the vector vorticity equation in place of the vorticity equation derived from secondary flow theory. Use of this equation would presumably reproduce the fully-developed results of Ghia and Sokhey. However, both approaches involve coordinate-related approximations, and it is not clear at this point which option would provide better flow predictions for developing flows. The differences observed in Fig. 6 are small and may be attributable in large part to differences in numerical truncation error, since different mesh distributions and grid points were used. In Fig. 7, an additional comparison is shown for the fully-developed primary flow velocity profile at the symmetry line midway between the two endwalls. Again, only minor differences between the present solution and that of Ghia and Sokhey are present. These differences presumably reflect the aforementioned differences in secondary flow velocity. Also shown in Fig. 7 are the experimental measurements of Mori, Uchida and Ukon [29], which do not agree well with either of the computed predictions. The disagreement between these measurements and various calculations for fully developed flow has not as yet been explained. Figures 8 and 9 contain the present predictions for primary and secondary velocity in the fully developed flow region.

Turbulent Duct Flow Comparison

The final test case consists of developing turbulent flow in the curved section of a 90° bend with straight extensions at the inlet and exit. This case was computed

for comparison with the recent experimental measurements of Taylor, Whitelaw, and Yianneskis [30] and has a curvature ratio R/H = 2.3, a Reynolds number Re_H of 40,000 and a Dean number of 26,370. The potential flow is not a free vortex for this geometry, because of the straight sections at the inlet and exit, although a free-vortex condition does occur near the center of the bend. For convenience in the present calculations, the potential flow pressure gradients were approximated by a streamwise distribution of free vortex flows with a variable centerline radius which is chosen such that the radial pressure difference between inner and outer radii of the bend matches that of an available potential flow calculation for this geometry (Humphrey, Taylor and Whitelaw [31]), and it is evident that the present approximation closely matches the transverse variation in streamwise pressure gradient present in the computed potential flow for this geometry.

The present calculation was initiated at the start of the bend with boundary layer thickness δ = 0.25H, chosen to match the experimental flow. Because the flow begins to turn upstream of the start of the bend, there is secondary flow present at the start of the calculation. This secondary flow was estimated from the Squire-Winter theory and corrected for no-slip conditions and continuity, as in the previous calculation at the Horlock, et al laminar flow. The transverse grid was locally refined near walls and consisted of 30 radial points and 20 points for the region between the endwall and symmetry plane. To reach the 77.5 degree position at which the last measurements in the curved duct were taken, 25 equally spaced axial steps were computed, and this required about 4 minutes of CDC 7600 run time.

Figures 11, 12 and 13 show comparisons at the 30°, 60° and 77.5° positions, respectively, of the predicted primary and secondary flow velocities and the measurements of Taylor, Whitelaw, and Yianneskis [30]. In general, the computed and measured velocity profiles are in very good agreement, except as noted below. The radial velocity profiles seem to be predicted extremely well, considering the difficulty of predicting strong turbulent secondary flows. It should be noted that the velocity profiles nearest both the pressure and suction surfaces ($\hat{r}$ = 0.1 and 0.9, respectively) are located well within the boundary layers on these surfaces, and are thus very sensitive to radial position. The only significant disagreement between the computed and measured velocity profiles occurs in the profiles nearest the suction side of the duct at the 60° and particularly the 77.5° locations (Figs. 12 and 13). In this region, there is considerable distortion of the primary flow as a result of the strong vortical secondary flow. The computed secondary flow structure consists of very strong radial flow within the endwall boundary layer and toward the inner wall

or suction surface of the duct, with radial velocity about 43 percent of the mean primary flow velocity. Upon reaching the suction surface, the secondary flow proceeds up the suction surface with peak velocity about 30 percent of the primary flow, and then near the symmetry plane is deflected away from the suction surface and back into the primary flow, forming a vortex structure. The radial flow near the symmetry plane is less concentrated than that near the walls and has a peak velocity of about 18 percent of the primary flow.

Since the primary flow is convected by the secondary flow, one effect of the strong secondary flow is to distort the primary flow, particularly near the suction surface. In Figs. 12 and 13, evidence of this primary flow distortion near the suction surface can be seen in both the present solution and in the experimental measurements, although agreement between the two is at best qualitative. The present computation predicts less distortion of the primary velocity near the suction surface than is present in the experimental measurements, particularly in Fig. 13a after 77.5 degrees of turning. This discrepancy may be due to approximations made in the analysis such as the treatment of streamwise pressure gradients or may represent a limitation of the turbulence model. Another possible explanation worthy of mention is numerical truncation error due to a large axial step size. The step size used in this calculation corresponds to a distance of 0.125H along the duct centerline and covers about 3 degrees of turning. Since the numerical algorithm employs a first-order backward difference formulation with "lagged" secondary velocities for the primary momentum and secondary vorticity equations, it may be expected that the computed solution would develop more slowly than the actual solution due to the first-order "lagging" truncation error. The computed results in Fig. 13a are consistent with this behavior, as was verified by comparing the computed primary flow velocity profile at $\hat{r} = 0.9$ and $\theta = 77.5$ degrees (Fig. 13a) with the corresponding measurements at $\theta = 60$ degrees (Fig. 12a). If the average free stream velocity is adjusted to reflect the difference in local static pressure, then the computed velocity profile for 77.5 degrees is in excellent agreement with the measured profile for 60 degrees. Further study including mesh refinement tests would be required to determine whether truncation error has significantly influenced the present comparisons - it is hoped that this mesh refinement study will be performed in the near future. Finally, in Fig. 14, the computed primary velocity profiles in the symmetry plane midway between the endwall surfaces are compared with the corresponding measurements. The level of agreement is the same as that present in Figs. 11-13.

SUMMARY AND CONCLUSIONS

(1) The present study includes further development and evaluation of the primary-secondary velocity decomposition approach suggested by Briley and McDonald [1] for application to viscous subsonic flow in smoothly curved geometries.

(2) An improved solution algorithm was developed here which provides for solution of the equations governing secondary vorticity and vector potential as a coupled system, using an iterative linearized block implicit (LBI) scheme. This permits implicit specification of no-slip boundary conditions for the secondary flow velocities and removes a previous assumption that flow in the near wall region is collateral. The present solution procedure is effective even with the extreme local mesh resolution which is necessary to resolve near-wall sublayer regions in turbulent flow calculations.

(3) Laminar flow calculations were made for specialized flow cases which would permit comparison with other experimental and analytical results. Secondary flows predicted by the present method were in good agreement with experimental measurements and a boundary layer similarity solution for a laminar flow in a strongly curved duct with thin boundary layers. This is a significant comparison and provides an indication that the present analysis adequately represents strong cross flows in thin boundary layers when they occur as a separate region of the flow distinct from corner flow regions.

(4) Although fully developed flows have little relevance in applications of interest here, the present prediction of a laminar fully developed flow agreed well with other fully developed solutions. This provides some validation of the approximations used in deriving the equation for secondary vorticity as an approximation of secondary flow theory.

(5) Predictions for turbulent flow in a strongly curved duct with moderate boundary layer thickness were compared with measured values of primary and secondary velocity. These flow conditions are typical of those occurring in turbomachinery applications of interest here. Considering the complexity of this flow, the agreement between predicted and measured velocity is very good except near the suction surface after considerable turning. In this region there is a strong corner vortex which results in considerable distortion of the primary flow. Although the corner vortex and primary flow distortion were

predicted in qualitative terms, further evaluation is necessary to determine the reason or reasons for the quantitative disagreement in this region.

(6) Overall, the present evaluation suggests that the initial value correction method used here does provide a reasonable description of the development of thin shear layers and secondary flows in strongly curved ducts. The method appears very promising as an economical procedure for making detailed predictions for this category of flow problems.

APPENDIX A:

GOVERNING EQUATIONS IN ORTHOGONAL COORDINATES

Velocity Decomposition

$$\bar{U} = \hat{i}_1 u_I u_v + \hat{i}_2 (v_I u_v + v_s) + \hat{i}_3 (w_I u_v + w_s) \tag{A-1}$$

$$v_s = \frac{1}{h_2} \frac{\partial \phi}{\partial x_2} + \frac{1}{h_1 h_3} \frac{\partial h_1 \psi}{\partial x_3} \tag{A-2}$$

$$w_s = \frac{1}{h_3} \frac{\partial \phi}{\partial x_3} - \frac{1}{h_1 h_2} \frac{\partial h_1 \psi}{\partial x_2} \tag{A-3}$$

Scalar Surface Potential ϕ

Eq. (8) is

$$\begin{aligned} &\frac{\partial}{\partial x_2} \rho \frac{h_1 h_3}{h_2} \frac{\partial \phi}{\partial x_2} + \frac{\partial}{\partial x_3} \rho \frac{h_1 h_2}{h_3} \frac{\partial \phi}{\partial x_3} \\ &= -\left[\frac{\partial}{\partial x_1} (h_2 h_3 \rho u_I u_v) + \frac{\partial}{\partial x_2} (h_1 h_3 \rho v_I u_v) \right. \\ &\qquad \left. + \frac{\partial}{\partial x_3} (h_1 h_2 \rho w_I u_v) \right] \end{aligned} \tag{A-4}$$

Vector Surface Potential ψ

Assuming $\nabla \times \bar{U}_I = 0$, Eq. (9) is

$$\begin{aligned} &\frac{1}{h_2 h_3} \left[\frac{\partial}{\partial x_2} \frac{\rho_o}{\rho} \frac{h_3}{h_1 h_2} \frac{\partial h_1 \psi}{\partial x_2} + \frac{\partial}{\partial x_3} \frac{\rho_o}{\rho} \frac{h_2}{h_1 h_3} \frac{\partial h_1 \psi}{\partial x_3} \right] \\ &= -\Omega_1 + \frac{v_I}{h_3} \frac{\partial u_v}{\partial x_3} - \frac{w_I}{h_2} \frac{\partial u_v}{\partial x_2} \end{aligned} \tag{A-5}$$

x_1 Momentum

$$\frac{u_1}{h_1}\frac{\partial u_1}{\partial x_1} + \frac{u_2}{h_1 h_2}\left[\frac{\partial h_1 u_1}{\partial x_2} - u_2\frac{\partial h_2}{\partial x_1}\right] + \frac{u_3}{h_1 h_3}\left[\frac{\partial h_1 u_1}{\partial x_3} - u_3\frac{\partial h_3}{\partial x_1}\right] + \frac{1}{h_1\rho}\frac{dp_v(x_1)}{dx_1} - \frac{1}{h_1}\frac{\partial}{\partial x_1}\left(\frac{q_I^2}{2}\right) = \frac{1}{\rho h_1 h_2 h_3}\left\{\frac{\partial}{\partial x_2}\left[\frac{h_3 h_1}{h_2}(\mu+\mu_T)\frac{\partial u}{\partial x_2}\right] + \frac{\partial}{\partial x_3}\left[\frac{h_1 h_2}{h_3}(\mu+\mu_T)\frac{\partial u}{\partial x_3}\right]\right\} \tag{A-6}$$

Second Vorticity

$$\left(\frac{u_1}{h_1}\frac{\partial}{\partial x_1} + \frac{u_2}{h_2}\frac{\partial}{\partial x_2} + \frac{u_3}{h_3}\frac{\partial}{\partial x_3}\right)\frac{\Omega_1}{\rho u_1} = -\frac{2}{\rho u_1}\left(\frac{\Omega_2}{h_1 h_2}\frac{\partial h_1}{\partial x_2} + \frac{\Omega_3}{h_1 h_3}\frac{\partial h_1}{\partial x_3}\right) - \frac{1}{h_2 h_3}\frac{1}{\rho^3 u_1^2}\left(\frac{\partial p_I}{\partial x_2}\frac{\partial \rho}{\partial x_3} - \frac{\partial p_I}{\partial x_3}\frac{\partial \rho}{\partial x_2}\right) + \frac{1}{h_2 h_3}\frac{1}{\rho u_1^2}\left(\frac{\partial}{\partial x_2}\left[\frac{h_3}{h_1 h_2 \rho}\frac{\partial h_1(\mu+\mu_T)\Omega_1}{\partial x_2}\right] + \frac{\partial}{\partial x_3}\left[\frac{h_2}{h_1 h_3 \rho}\frac{\partial h_1(\mu+\mu_T)\Omega_1}{\partial x_3}\right]\right) \tag{A-7}$$

The transverse vorticity components are given by

$$\Omega_2 = \hat{i}_2 \cdot \nabla \times \bar{U} = \frac{u_I}{h_3}\frac{\partial u_v}{\partial x_3} - \frac{w_I}{h_1}\frac{\partial u_v}{\partial x_1} - \frac{1}{h_1 h_3}\frac{\partial}{\partial x_1}(h_3 w_s) \tag{A-8}$$

$$\Omega_3 = \hat{i}_3 \cdot \nabla \times \bar{U} = -\frac{u_I}{h_2}\frac{\partial u_v}{\partial x_2} + \frac{v_I}{h_1}\frac{\partial u_v}{\partial x_1} + \frac{1}{h_1 h_2}\frac{\partial}{\partial x_1}(h_s v_s) \tag{A-9}$$

Pressure Gradient Relation

Eq. (26) is given by

$$\frac{1}{h_1}\frac{\partial}{\partial x_1}\left[\frac{\gamma-1}{\gamma}\rho\left(E-\frac{q^2}{2}\right)-p_I-p_v(x_1)\right]=0 \tag{A-10}$$

where

$$\hat{i}\cdot\left[\nabla p_I+\rho\nabla(q_I^2/2)\right]=0 \tag{A-11}$$

Energy Equation

To simplify the energy equation, assumptions are made which are appropriate for boundary layer flow on walls aligned with either an $x_1 - x_2$ surface or an $x_1 - x_3$ surface. Eq. (24) can then be approximated by

$$\frac{\rho u_1}{h_1}\frac{\partial E}{\partial x_1}+\frac{\rho u_2}{h_2}\frac{\partial E}{\partial x_2}+\frac{\rho u_3}{h_3}\frac{\partial E}{\partial x_3}$$

$$=\frac{1}{h_1h_2h_3}\left\{\frac{\partial}{\partial x_2}\left[\left(\frac{\mu}{Pr}+\frac{\mu_T}{Pr_t}\right)\frac{h_1h_3}{h_2}\frac{\partial E}{\partial x_2}+\frac{h_1h_3}{2h_2}\left(\mu\left(1-\frac{1}{Pr}\right)+\mu_T\left(1-\frac{1}{Pr_t}\right)\right)\frac{\partial}{\partial x_2}(u_1^2+u_3^2)\right]\right.$$

$$\left.+\frac{\partial}{\partial x_3}\left[\left(\frac{\mu}{Pr}+\frac{\mu_T}{Pr_t}\right)\frac{h_1h_2}{h_3}\frac{\partial E}{\partial x_3}+\frac{h_1h_2}{2h_3}\left(\mu\left(1-\frac{1}{Pr}\right)+\mu_T\left(1-\frac{1}{Pr_t}\right)\right)\frac{\partial}{\partial x_3}(u_1^2+u_2^2)\right]\right. \tag{A-12}$$

where the Prandtl number Pr is defined by $Pr = c_p\mu/k$, and Pr_t is the turbulent Prandtl number.

APPENDIX B:

TURBULENCE MODEL

In turbulent flow applications, the stress terms F' and G' in Eqs. (15), (20), and (22) contain turbulent shear stresses in the form of fluctuating velocity and velocity-temperature correlations. In the present application to flow in curved ducts, these turbulent stresses are modeled by introduction of an effective turbulent eddy viscosity whose distribution is determined by solution of turbulence-model equations. The present treatment employs the one-equation turbulence model developed by Shamroth and Gibeling [32]. This model is based upon the turbulence energy partial differential equation, an algebraic length scale equation and a relation between dissipation, turbulence energy, and the length scale of the form $\epsilon = C_\mu^{3/4} k^{3/2}/\ell$ where C_μ is a turbulence structural coefficient. To calculate low Reynolds number or transitional flows, C_μ is made a function of the turbulent Reynolds number. The length scale is determined from a mixing length distribution appropriate for the flow under consideration. This turbulence model is related to two-equation models as discussed by Launder and Spalding [33], since both models solve a form of the turbulence kinetic energy equation. The major difference is that the one-equation model replaces assumptions necessary to solve the turbulence dissipation equation with assumptions regarding the length scale formulation. In the present application, the length scale is determined from solution of a momentum integral equation which serves to model the streamwise development of a freestream length scale, and from a prescribed length scale distribution in cross-sectional planes.

Using Cartesian tensor notation and overbars to indicate time averaging the turbulence kinetic energy is defined as

$$k = \frac{1}{2} \overline{u_i' u_i'} \tag{B-1}$$

and the turbulence dissipation is

$$\epsilon = \nu \overline{\frac{\partial u_i'}{\partial x_j} \frac{\partial u_i'}{\partial x_j}} \tag{B-2}$$

The low Reynolds number form of the transport equation for the turbulence kinetic energy is given [33] as

$$\rho U \cdot \nabla k = \nabla \cdot (\mu + \mu_T/\sigma_k) \nabla k + P - 2\mu \nabla K^{1/2} \cdot \nabla K^{1/2} - \rho\epsilon \tag{B-3}$$

where P is the turbulent production. The constant, σ_k is taken as 1.0 as recommended by Launder and Spalding [33]. By hypotheses, Prandtl and Kolmogorov has suggested that the effective viscosity is proportional to the local density and the product of a characteristic turbulent velocity and length scale. The characteristic velocity is assumed equal to the square root of the local value of turbulence kinetic energy, thus

$$\mu_T = C \rho \ell K^{1/2} \tag{B-4}$$

where c is a constant of proportionality. Through dimensional arguments, the length scale may be related to the turbulent kinetic energy and dissipation as

$$\ell = C^3 k^{3/2}/\epsilon \tag{B-5}$$

Based on an examination of a large amount of experimental data Launder [33] has recommended that $c^4 = 0.09 \equiv c_\mu$, and under these conditions the length scale may be thought of as the conventional mixing length. Using Eq. (5) the turbulence kinetic energy equation may be expressed as

$$\rho U \cdot \nabla k = \nabla \cdot (\mu + \mu_T/\sigma_k) \nabla k + P - 2\mu \nabla K^{1/2} \cdot \nabla K^{1/2} - \rho C_\mu^{3/4} K^{3/2}/\ell \tag{B-6}$$

For near wall and low Reynolds number flows, c_μ is modified by a damping factor. Following Shamroth and Gibeling [32], a turbulence function is defined such that

$$C_\mu = 4a_1^2 \tag{B-7}$$

where a_1 is a function of a turbulent Reynolds number originally derived by McDonald and Fish [34] for transitional boundary layer flows,

$$a_1 = a_0 \left[\frac{f(R_T)}{100} \right] \Bigg/ \left\{ 1.0 + 6.66\, a_0 \left[\frac{f(R_T)}{100} - 1 \right] \right\} \tag{B-8}$$

In Eq. (B-8), a_0 is taken as 0.0115 R_T is the turbulent Reynolds number, and the function $f(R_T)$ is given as [34]

$$f(R_T) = 100.\, R_T^{0.22} \qquad R_T \le 1$$

$$f(R_T) = 68\,1 R_T + 614.3 \qquad R_T \ge 40 \tag{B-9}$$

Between the limits of $1<R_T<40$ a cubic is used to join the two functional forms given by Eq. (B-9). In [34], the turbulent Reynolds number, R_T, was defined as an integral average across the boundary layer. Here, the low Reynolds number variation of a_1 relates to the near wall region rather than to transition from laminar to turbulent flow, and R_T is thus taken as the local ratio of turbulent to laminar viscosity,

$$R_T = \frac{\mu_T}{\mu} \tag{B-10}$$

Use of the one-equation turbulence model requires specification of a length scale distribution appropriate for the problem under consideration. The duct flows of interest here are presumed to have moderately thin shear layers on the boundary walls, and the length scale distribution is thus adapted from previous turbulence models for turbulent boundary layers. The mixing length distribution of McDonald and Fish [34] is one which has proven effective for a wide range of two-dimensional turbulent boundary layers and is easily adapted for present use. This distribution is given by

$$\ell = \mathcal{D}\ell_\infty \tanh(\kappa\, d/\ell_\infty) \tag{B-11}$$

where ℓ is mixing length, ℓ_∞ is a free stream mixing length, d is distance from the wall, k is the von Karman constant (taken as 0.43), and $\mathcal{D}$ is a sublayer damping function given by

$$\mathcal{D} = P^{1/2}\left[(d^+ - 23)/8\right] \tag{B-12}$$

Here, P is the normal probability function and d^+ is defined by $d^+ = d\,(\tau/\rho)^{1/2}/\nu$, where τ is shear stress. For equilibrium boundary layers, ℓ_∞ is about 0.09 δ, where δ is the boundary layer thickness.

The length distribution of Eq. (B-11) is adapted for present use by taking d as distance to the nearest wall and by assigning ℓ_∞ a representative value at each streamwise location in the duct, taken as 0.09 δ_e where δ_e is a representative boundary layer thickness. The only remaining difficulty is to determine a suitable value of δ_e. Since shear layers occur on all surfaces and in corner regions, and since the

free stream primary flow is subject to considerable distortion, it does not appear feasible to determine a mean boundary layer thickness from the cross-sectional variation of the primary flow velocity. Instead, at the starting location, an "effective" boundary layer thickness is defined as

$$\delta_e = \frac{\sum_i \delta_i \ell_i}{\sum_i \ell_i} \tag{B-13}$$

where δ_i is the initial boundary layer thickness on "i"th wall, and ℓ_i is the length of the "i"th wall of the duct. The boundary layer thickness is then assumed to grow in accordance with the momentum integral equation for a two-dimensional boundary layer. Assuming a 1/7 power law velocity profile and a pipe flow skin friction law consistent with the 1/7 power velocity profile (cf. Schlichting [35]), the momentum integral equation can be written as

$$\frac{7}{72}\frac{d\delta_e}{dx} + \frac{23}{72}\frac{\delta_e}{u_\infty}\frac{du_\infty}{dx} = 0.0225\left(\frac{\nu}{u_\infty \delta_e}\right)^{1/4} \tag{B-14}$$

The free stream velocity gradient du_∞/dx in Eq. (B-14) is determined from the mean pressure drop predicted as the forward-marching calculation proceeds. Eq. (B-14) is then solved to obtain δ_e, and the free stream mixing length is taken as $\ell_\infty = 0.09\ \delta_e$. With the length distribution then available from Eq. (B-11), the turbulence kinetic energy equation (B-6) is solved, and the turbulent viscosity is determined from Eq. (B-4).

REFERENCES

1. Briley, W. R. and McDonald, H.: Analysis and Computation of Viscous Subsonic Primary and Secondary Flows. AIAA Paper No. 79-1453, July, 1979.

2. Hawthorne, W. R.: The Applicability of Secondary Flow Analyses to the Solution of Internal Flow Problems", Fluid Mechanics of Internal Flow, ed. G. Sovran, (Elsevier), 1967, p. 263.

3. Hawthorne, W. R.: "Research Frontiers in Fluid Dynamics", eds. R. J. Seeger and G. Temple, (Interscience), 1965, p. 1.

4. Horlock, J. H. and Lakshminarayana, B.: "Secondary Flows; Theory, Experiment and Application in Turbomachinery Aerodynamics", Annual Rev. Fluid Mech., Vol. 5, 1973, p. 247.

5. Rowe, M.: "Measurements and Computations of Flow in Pipes", J. Fluid Mech., Vol. 43, 1970, p. 771.

6. Lakshminarayana, B. and Horlock, J. H.: "Generalized Expressions for Secondary Vorticity Using Intrinsic Coordinates", J. Fluid Mech., Vol. 59, 1973, p. 97.

7. Briley, W. R. and McDonald, H.: "On the Structure and Use of Linearized Block ADI and Related Schemes", J. Comp. Phys., Vol. 34, 1980, p. 54.

8. Briley, W. R. and McDonald, H.: "Computation of Three-Dimensional Horseshoe Vortex Flow Using the Navier-Stokes Equations", Seventh International Conference on Numerical Methods in Fluid Dynamics, Stanford Univ. and NASA/Ames, June, 1980.

9. Patankar, S. V. and Spalding, D. B.: "A Calculation Procedure for Heat, Mass, and Momentum Transfer in Three-dimensional Parabolic Flows", Int. J. Heat and Mass Transfer, Vol. 15, 1972, p. 1787.

10. Caretto, L. S., Curr, R. M., Spalding, D. B.: "Two Numerical Methods for Three-Dimensional Boundary Layers", Comp. Methods in Appl. Mech. and Engr., Vol. 1, 1973, p. 39.

11. Briley, W. R.: "Numerical Method for Predicting Three-dimensional Steady Viscous Flow in Ducts", J. Comp. Phys., Vol. 14, 1974, p. 8.

12. Ghia, K. N. and Sokhey, J. S.: "Laminar Incompressible Viscous Flow in Curved Ducts of Rectangular Cross-Sections", J. Fluids Engr., Vol. 99, 1977, p. 640.

13. Rubin, S. C. and Khosla, P. K.: "Laminar Flow in Rectangular Channels, Part II - Numerical Solution for a Square Channel", Computer Methods in Fluid Mech., ASME, 1976, p. 29.

14. Shamroth, S. J. and Briley, W. R.: "A Viscous Flow Analysis of the Tip Vortex Generation Process", AIAA Paper No. 79-1546, 1979.

15. Kreskovsky, J. P., Briley, W. R. and McDonald, H.: "Development of a Method for Computing Three-Dimensional Subsonic Viscous Flows in Turbofan Lobe Mixers", SRA Report R78-300002-12, Nov., 1978.

16. Anderson, B. H., Povinelli, L. A. and Gerstenmaier, W.: "Influence of Pressure Driven Secondary Flows on the Behavior of Turbofan Forced Mixers", AIAA Paper 80-1198, 1980.

17. Levy, R., McDonald, H., Briley, W. R. and Kreskovsky, J. P.: "A Three-Dimensional Turbulent Compressible Subsonic Duct Flow Analysis for Use with Constructed Coordinate Systems", AIAA Paper 80-1398, 1980.

18. Pratap, V. S. and Spalding, D. B.: "Fluid Flow and Heat Transfer in Three-Dimensional Duct Flows", Int. J. Heat & Mass Transfer, Vol. 19, 1976, p. 1183.

19. Moore, J. and Moore, J. G.: "A Calculation Procedure for Three-Dimensional Viscous, Compressible Duct Flow. Parts I and II", J. of Fluid Engr., Vol. 101, 1979, p. 415.

20. Dodge, P. R.: "A Numerical Method for 2-D and 3-D Viscous Flows", AIAA Paper No. 76-425, 1976.

21. Dwoyer, D. L.: "Application of a Velocity-Split Navier-Stokes Solution Technique to External Flow Problems", AIAA Paper 79-1449, 1979.

22. Shapiro, A. H.: "The Dynamics and Thermodynamics of Compressible Fluid Flow", Vol. I, (Ronald Press), 1955.

23. Lieblein, S. and Stockman, N. O.: "Compressibility Correction for Internal flow Solutions", J. Aircraft, Vol. 9, 1971, p. 312.

24. Roberts, G. O.: "Computational Meshes for Boundary Layer Problems", Proc. 2nd Int. Conf. Num. Meth. Fluid Dynamics, (Springer-Verlag), 1971, p. 171.

25. Ralston, A: "A First Course in Numerical Analysis", (McGraw-Hill), 1965, p. 323.

26. Horlock, J. H., Lewkowicz, A. K. and Wordsworth, J.: "Three-Dimensional Laminar Boundary Layers in Crosswise Pressure Gradients", J. Fluid Mech., Vol. 66, 1974, p. 641.

27. Horlock, J. H. and Wordsworth, J.: "The Three-Dimensional Laminar Boundary Layer on a Rotating Helical Blade", J. Fluid Mech., Vol. 23, 1965, p. 305.

28. Squire, H. B. and Winter, K. G.: "The Secondary Flow in a Cascade of Airfoils in a Non-Uniform Stream", J. Aero. Sci., Vol. 18, 1951, p. 271.

29. Mori, Y., Uchida, Y. and Ukon, T.: "Forced Convective Heat Transfer in a Curved Channel with a Square Cross Section", Int. J. Heat and Mass Transfer, Vol. 14, 1971, p. 1782.

30. Taylor, A. M. K. P., Whitelaw, J. H. and Yianneskis, M.: "Measurements of Laminar and Turbulent Flow in a Curved Duct with Thin Inlet Boundary Layers", Report FS/80/29, ME Dept. Imperial College of Science and Technology, 1980.

31. Humphrey, J. A. C., Taylor, A. M. K. and Whitelaw, J. H.: "Laminar Flow in a Square Duct of Strong Curvature", J. Fluid Mech., Vol. 83, 1977, p. 509.

32. Shamroth, S. J. and Gibeling, H. J.: "The Prediction of the Turbulent Flow Field about an Isolated Airfoil", AIAA Paper 79-1543, 1979.

33. Launder, B. E. and Spalding, D. B.: "The Numerical Computation of Turbulent Flows", Computer Methods in Applied Mechanics and Engineering, Vol. 3, 1974, p. 269.

34. McDonald H. and Fish, R. W.: "Practical Calculations of Transitional Boundary Layers", Int. J. Heat and Mass Transfer, Vol. 16, 1979, p. 1729.

35. Schlichting, H.: "Boundary Layer Theory", (McGraw-Hill), New York, 1960.

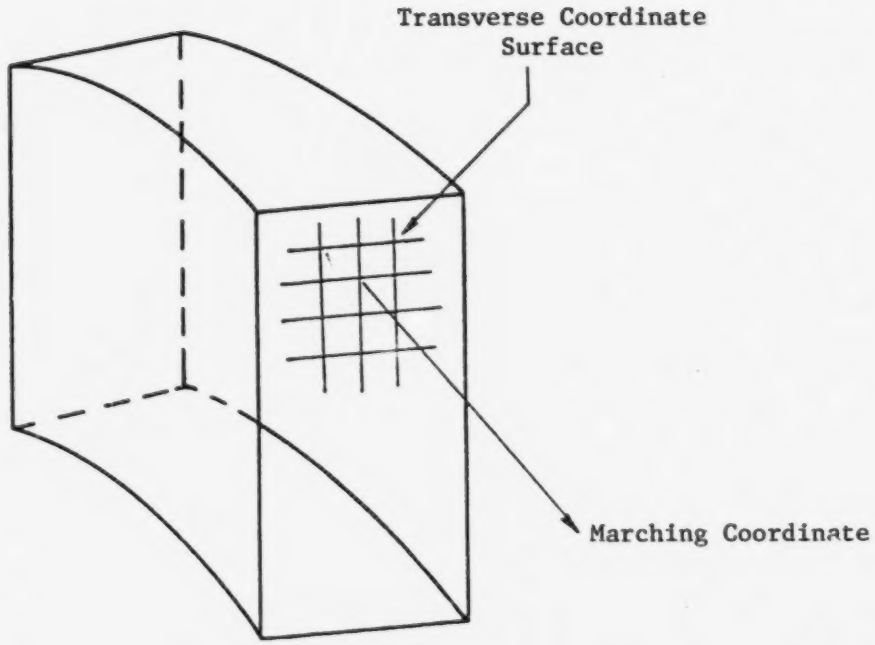

Fig. 1 - Schematic of Coordinate System for
Three-Dimensional Flow Problem.

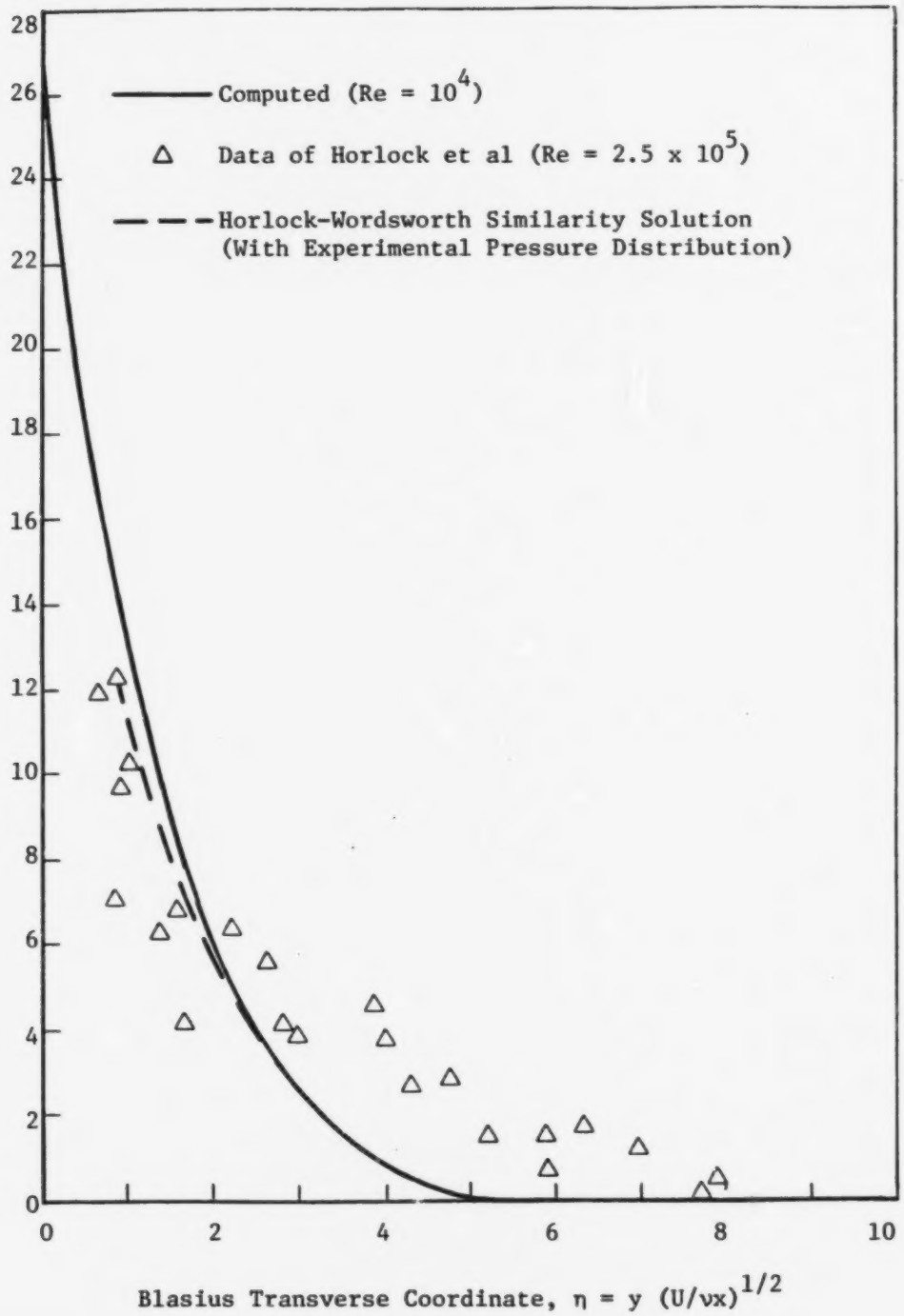

Fig. 2 - Yaw Angle Profile for a Circular Arc Duct of Rectangular Cross Section, R/H=3.5, X=0.75 H.

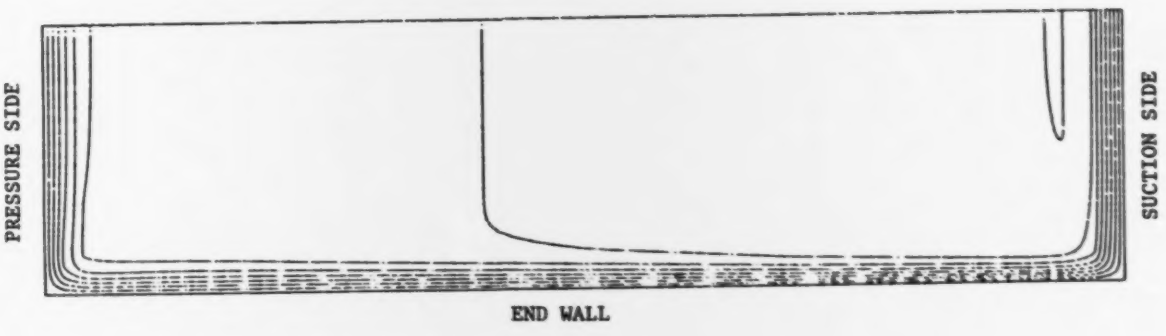

a. Primary Flow Velocity Contours

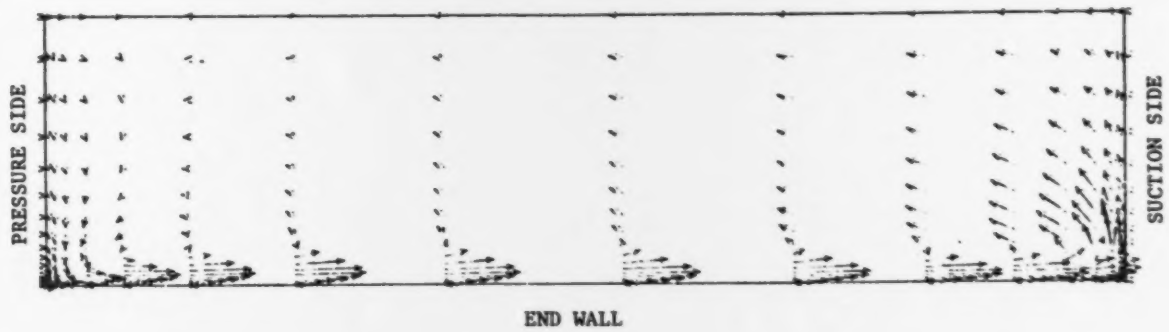

b. Secondary Flow Velocity Vectors

Fig. 3 - Computed Results for Circular Arc Duct, $Re=10^4$, R/H=3.5 at Measuring Station of Horlock et al.

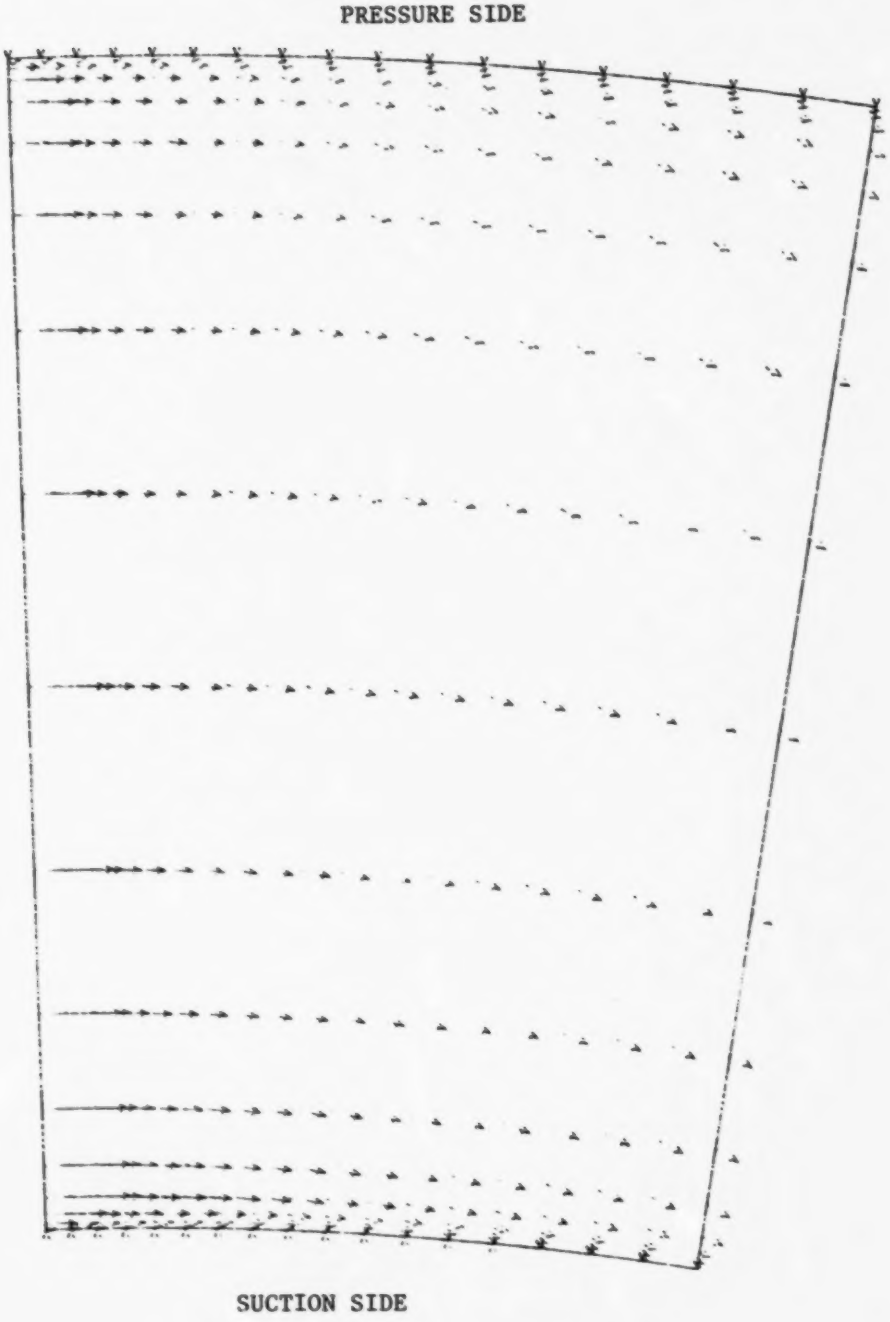

Fig. 4 - Flow in a Plane One Grid Point Away from Endwall Circular Arc Duct, $Re=10^4$, R/H=3.5.

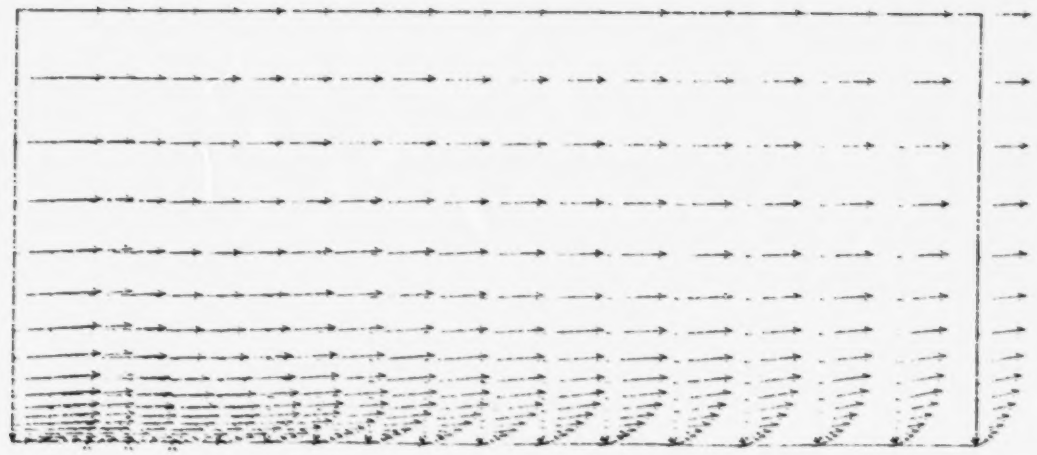

a. Inner (suction) Surface

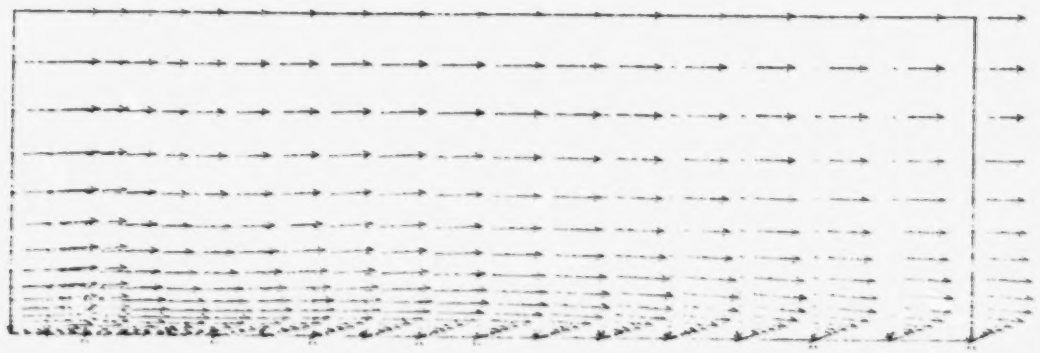

b. Outer (pressure) Surface

Fig. 5 - Flow in Surfaces One Grid Point Away from Sidewalls ("unwrapped" to lie in a plane).

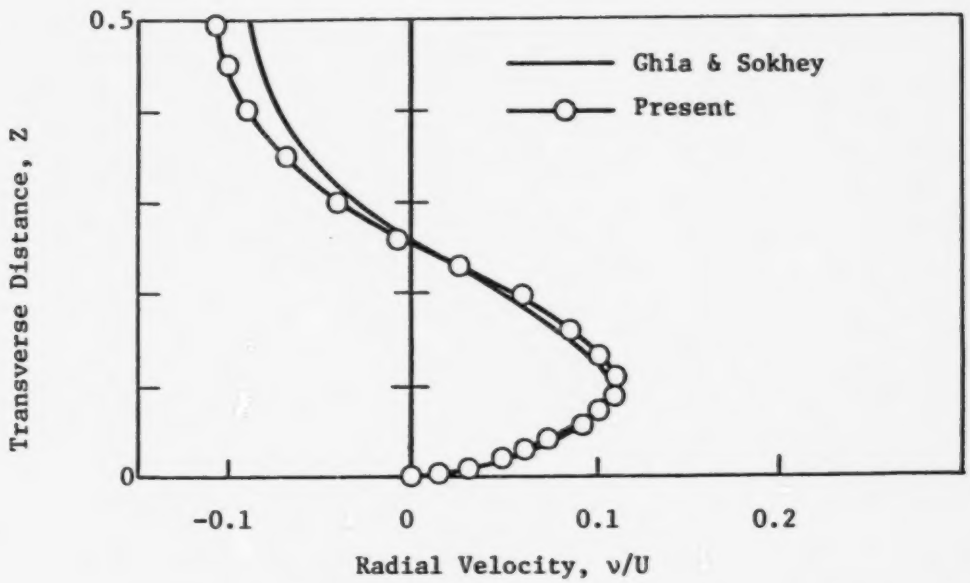

Fig. 6 - Fully Developed Radial Velocity Profile at r=0.4 for a Circular Arc Duct of Square Cross Section, R/H=14, Re=205, K=55.

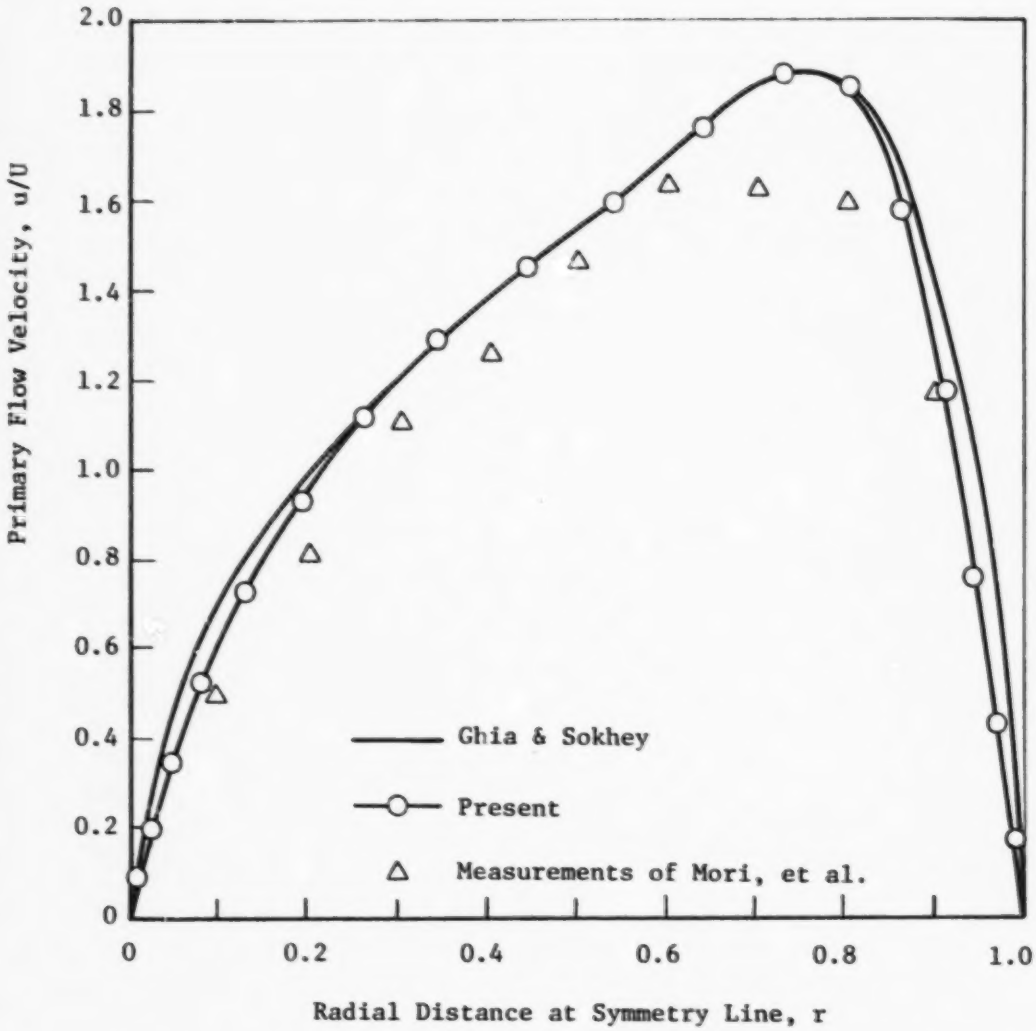

Fig. 7 - Fully Developed Primary Flow Velocity Profile for a Circular Arc Duct of Square Cross Section, R/H=14, Re=205, K=55.

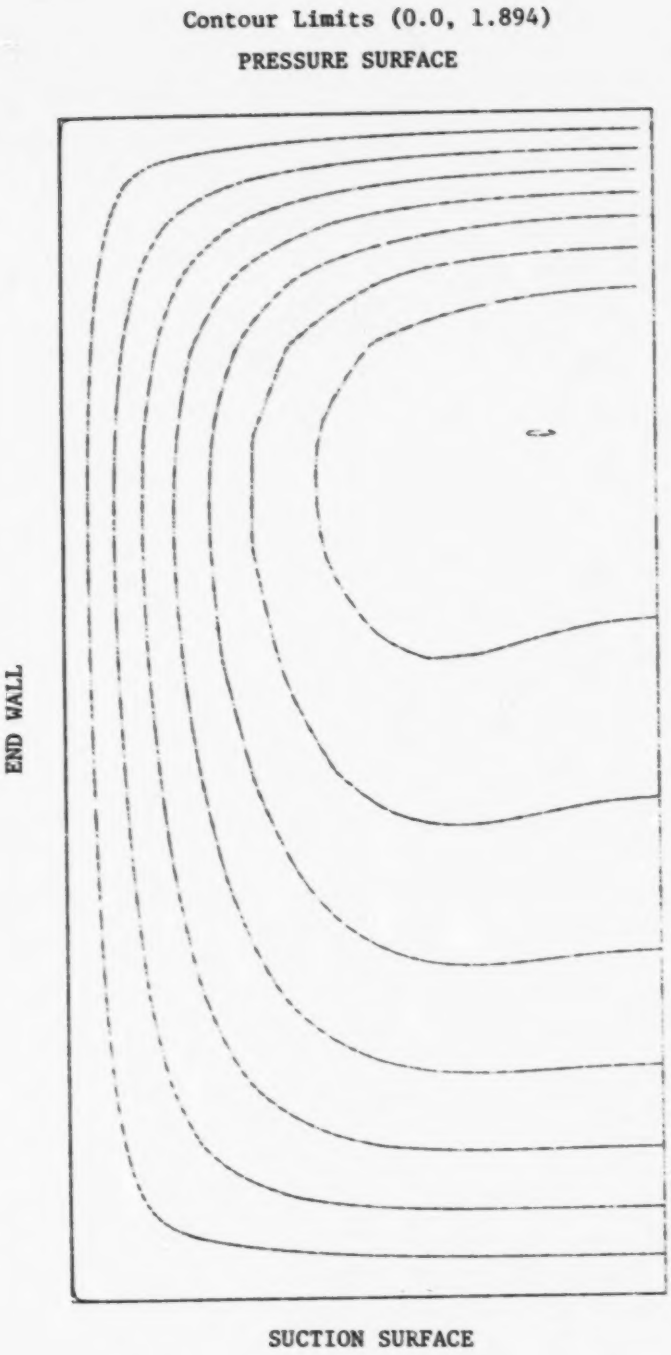

Fig. 8 - Primary Flow Velocity Contours for Fully Developed Circular Arc Duct, Re=205, R/H=14, K=55.

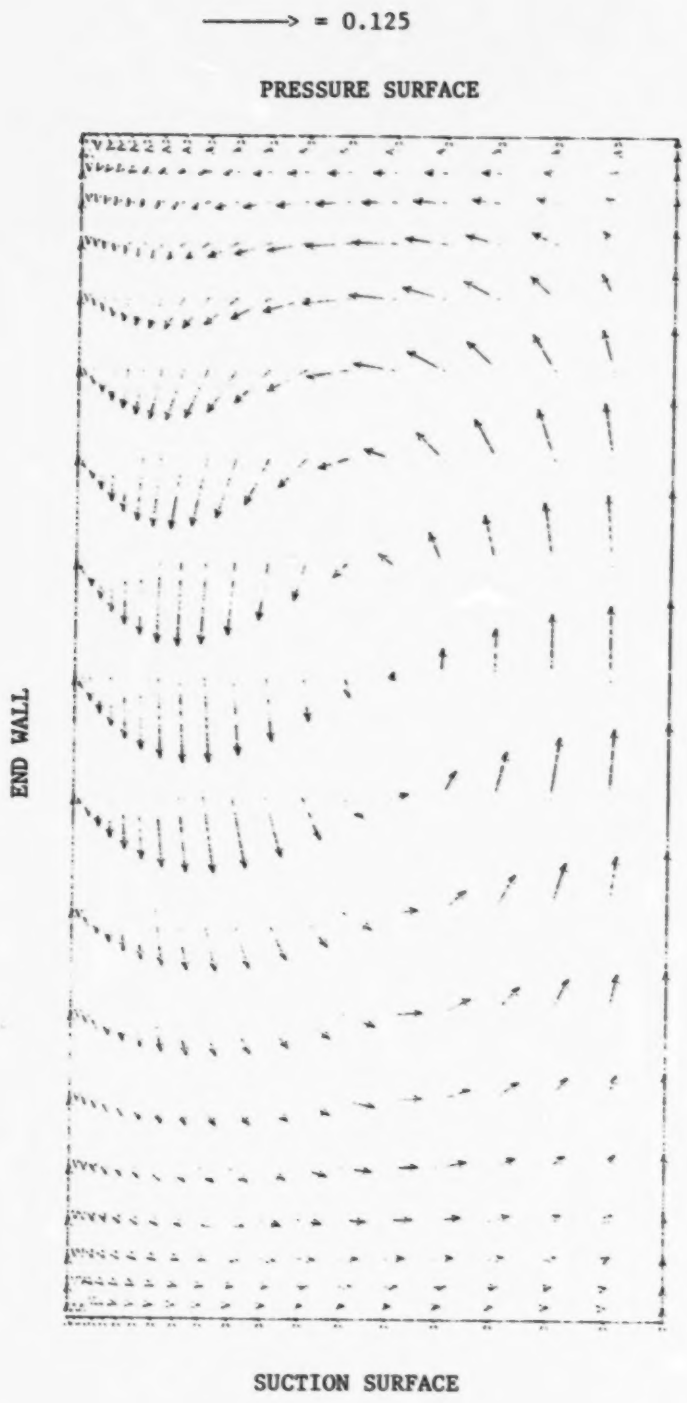

Fig. 9 - Secondary Velocity for Fully Developed Circular Arc Duct Re=205, R/H=14, K=55.

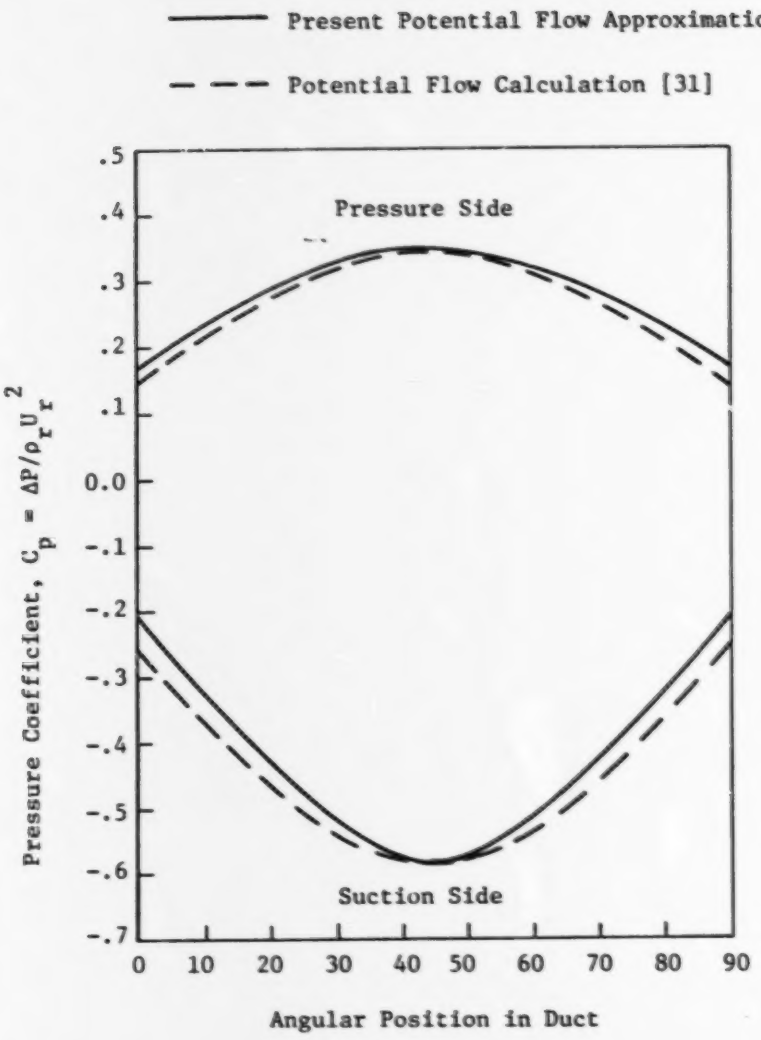

Fig. 10 - Comparison of Approximate Potential Flow Pressure Distribution with Computed Solution.

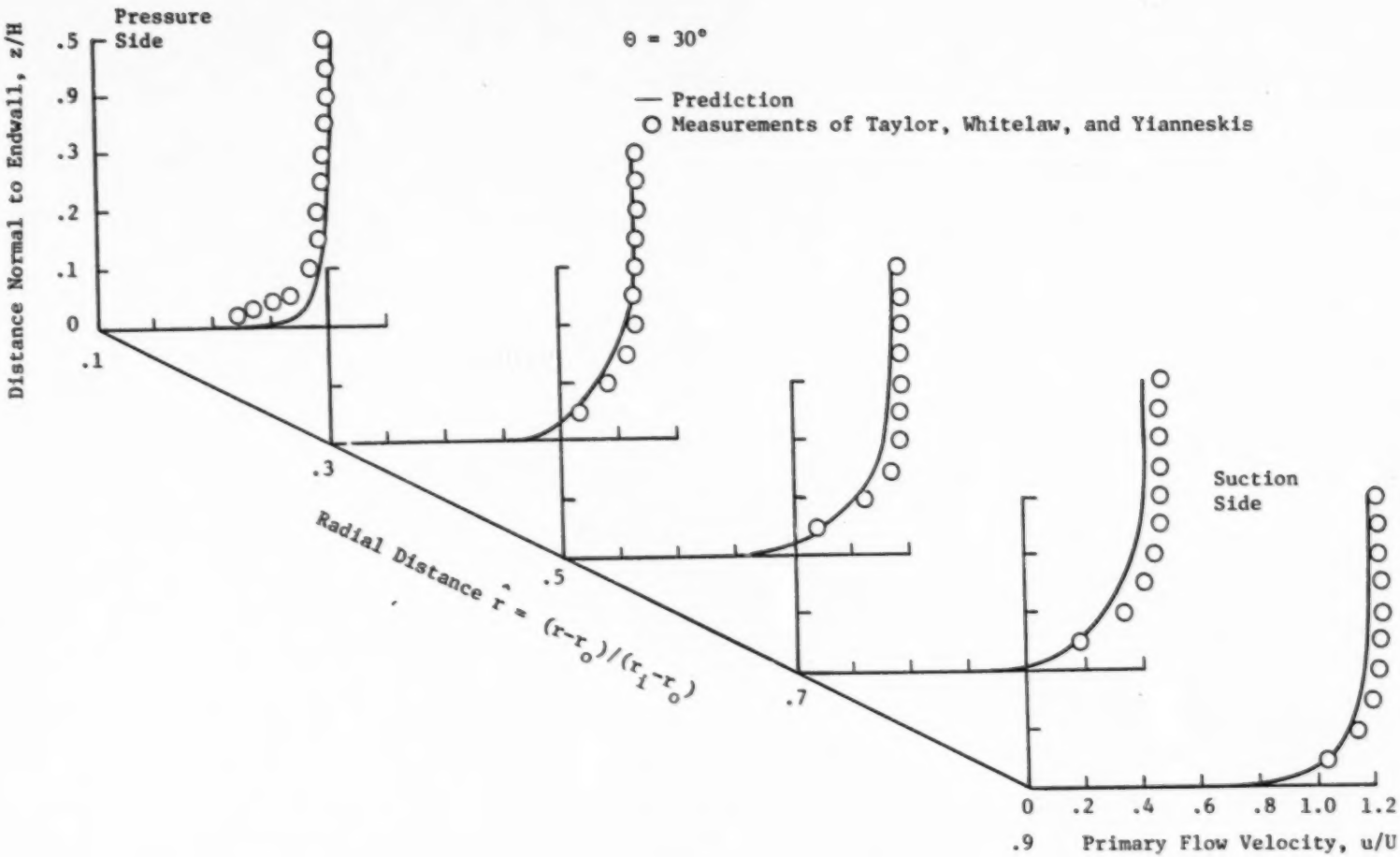

Fig. 11a - Primary Flow Velocity Profiles After 30 Degrees of Turning in a Circular Arc Duct of Square Crossection, R/H=2.3, Re=40000, k=26370.

BLANK PAGE

BLANK PAGE

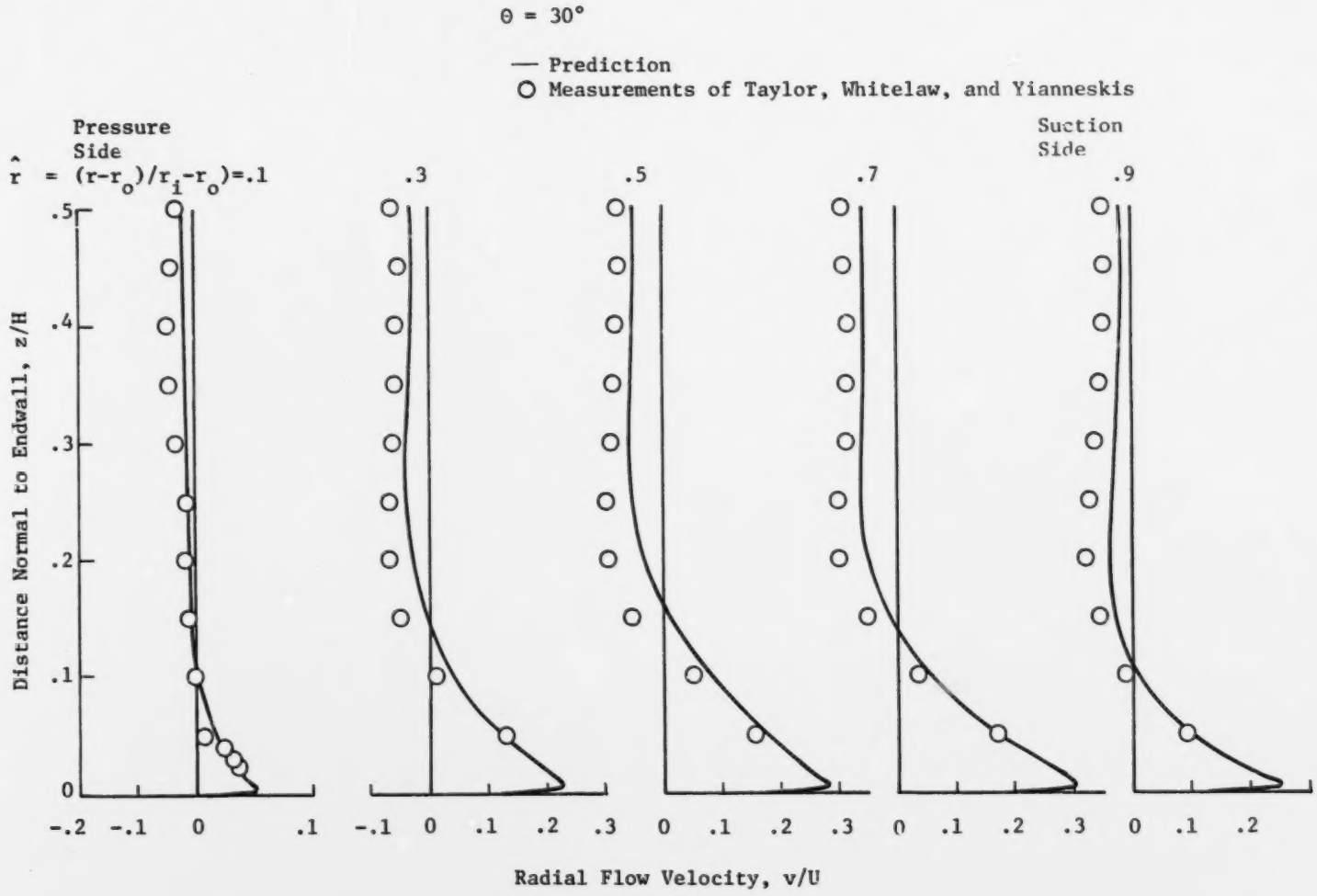

Fig. 11b - Radial Flow Velocity Profiles After 30 Degrees of Turning in a Circular Arc Duct of Square Crossection, R/H=2.3, Re=40000, k=26370.

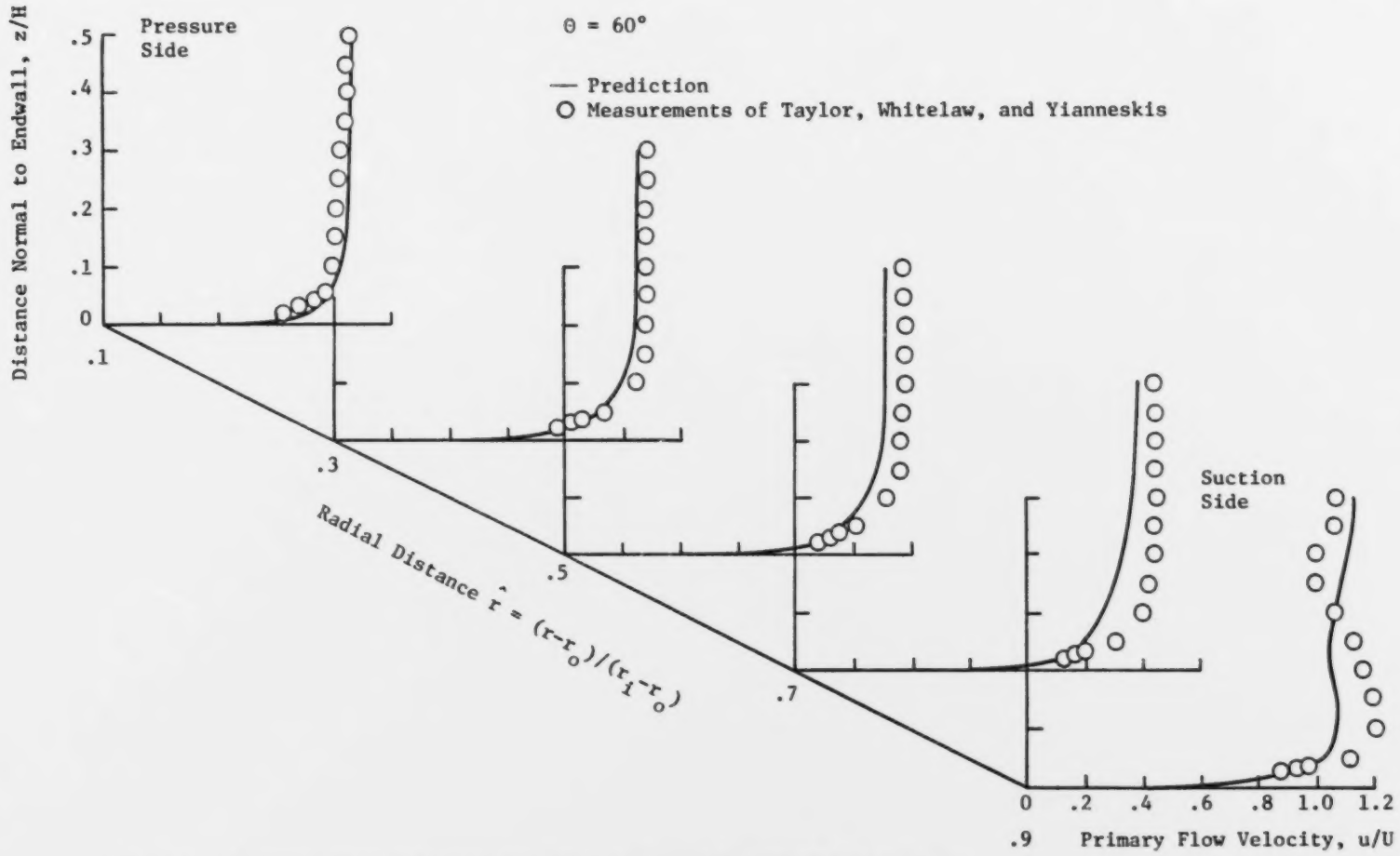

Fig. 12a - Primary Flow Velocity Profiles After 60 Degrees of Turning in a Circular Arc Duct of Square Crossection, R/H=2.3, Re=40000, k=26370.

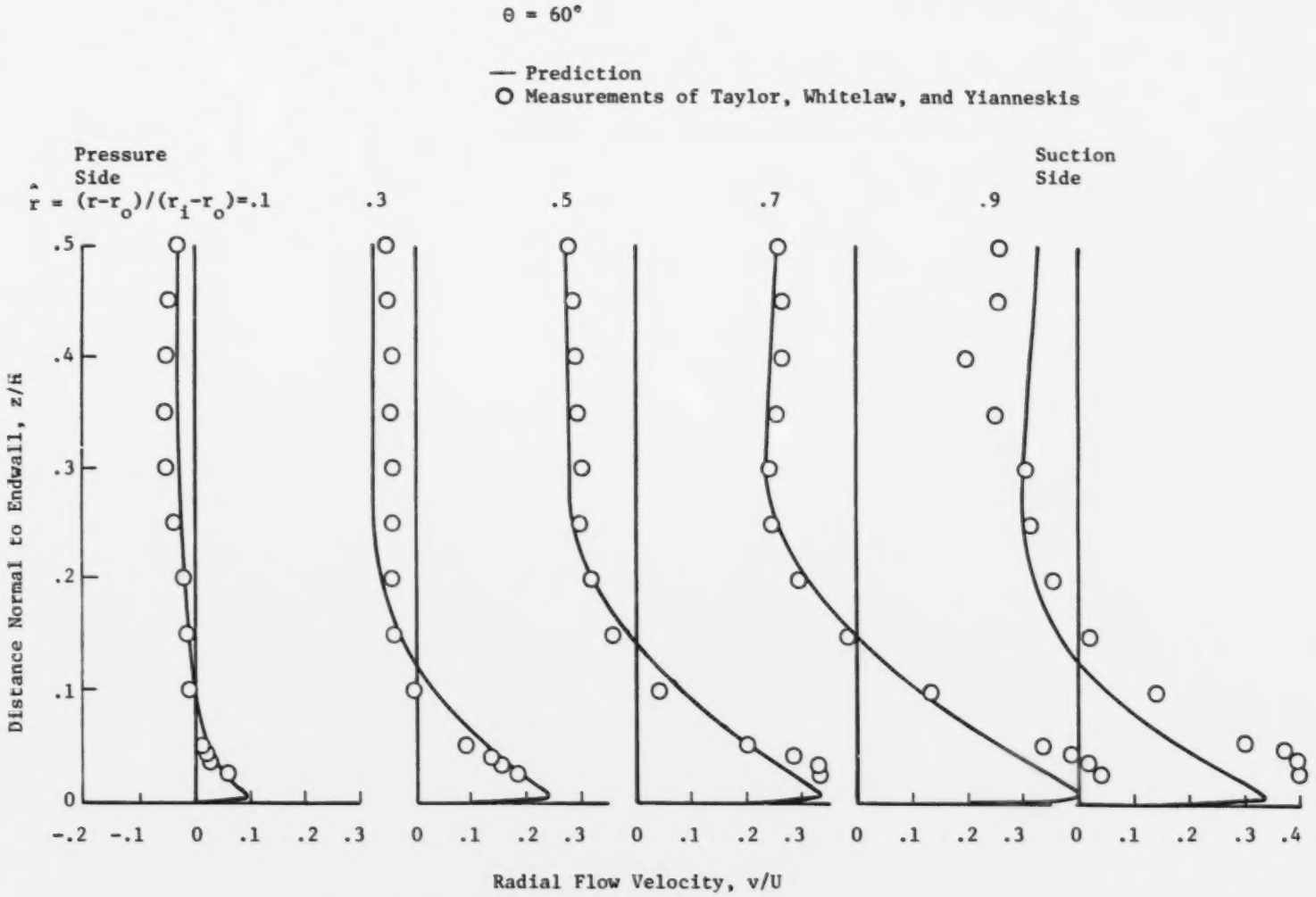

Fig. 12b- Radial Flow Velocity Profiles After 60 Degrees of Turning in a Circular Arc Duct of Square Crossection, R/H=2.3, Re=40000, k=26370.

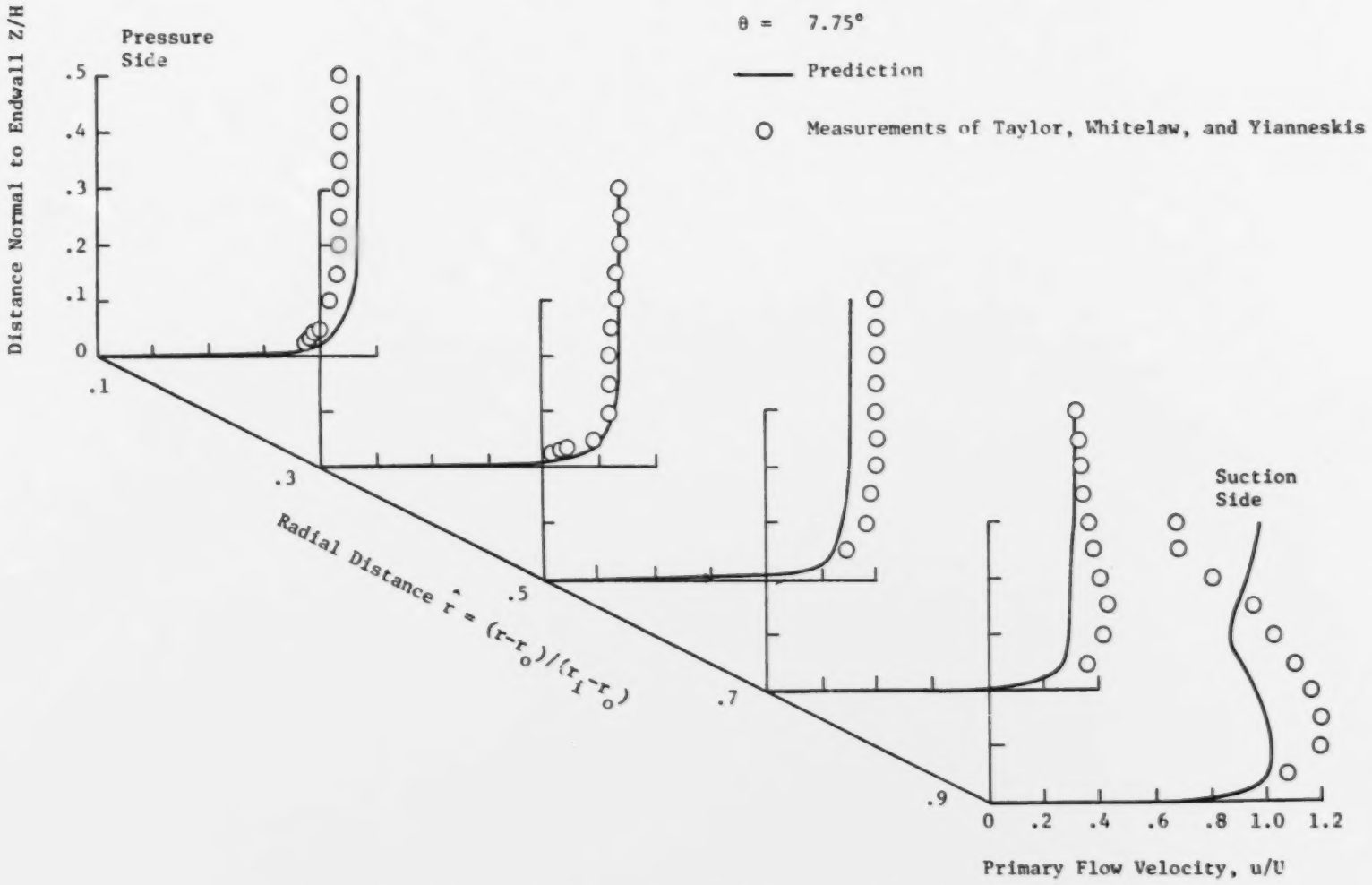

Fig. 13a - Primary Flow Velocity Profiles After 77.5 Degrees of Turning in a Circular Arc Duct of Square Crossection, R/H=2.3, Re=40000, K=26370.

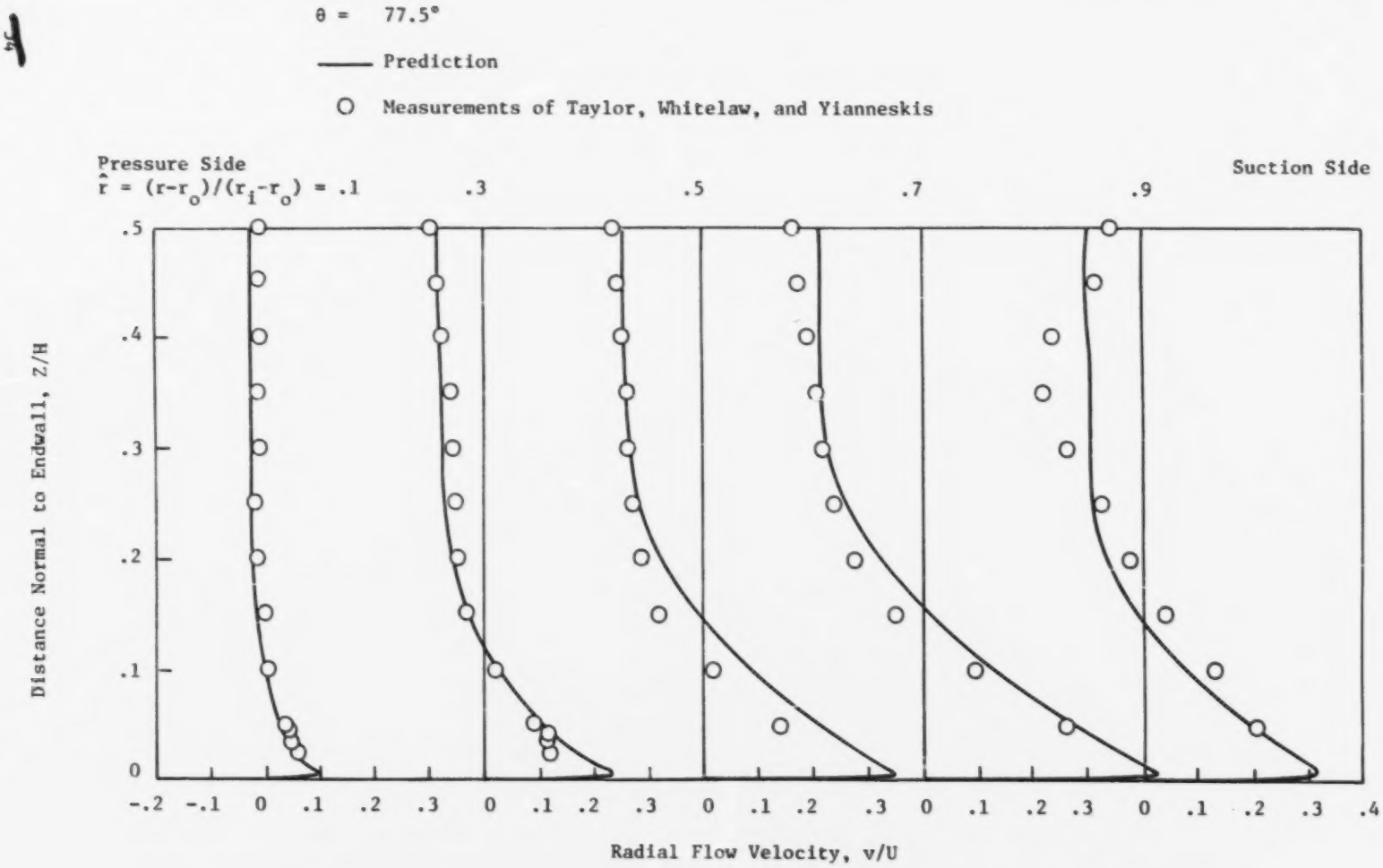

Fig. 13b - Radial Flow Velocity Profiles After 77.5 Degrees of Turning in a Circular Arc Duct of Square Crossection, R/H=2.3, Re=40000, K=26370.

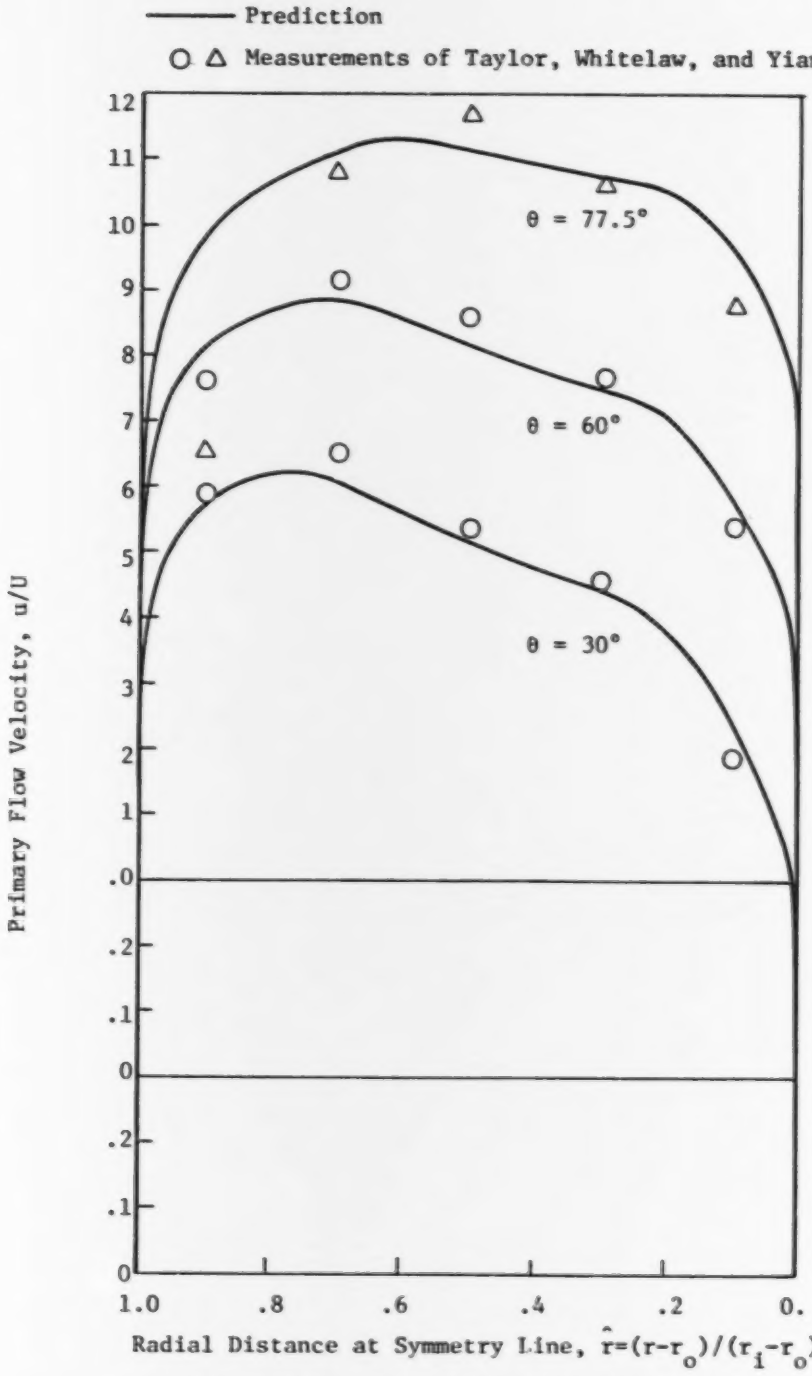

Fig. 14 - Primary Flow Velocity Profiles at 30 and 60 Degrees in a Circular Arc Duct of Square Crossection, R/H=2.3, Re=40000, K=26370.

1. Report No. NASA CR-3388	2. Government Accession No.	3. Recipient's Catalog No.
4. Title and Subtitle PREDICTION OF LAMINAR AND TURBULENT PRIMARY AND SECONDARY FLOWS IN STRONGLY CURVED DUCTS		5. Report Date February 1981 6. Performing Organization Code
7. Author(s) J. P. Kreskovsky, W. R. Briley, and H. McDonald		8. Performing Organization Report No. R80-900007-12 10. Work Unit No.
9. Performing Organization Name and Address Scientific Research Associates, Inc. Box 498 Glastonbury, Connecticut 06033		11. Contract or Grant No. NAS3-22014 13. Type of Report and Period Covered Contractor Report
12. Sponsoring Agency Name and Address National Aeronautics and Space Administration Washington, D.C. 20546		14. Sponsoring Agency Code 532-06-12

15. Supplementary Notes

Final report. Project Manger, Eric R. McFarland, Fluid Mechanics and Acoustics Division, NASA Lewis Research Center, Cleveland, Ohio 44135.

16. Abstract

Numerical solutions are presented for three-dimensional laminar and turbulent flow in curved ducts of rectangular cross section and significant curvature. The analysis is based on a primary-secondary velocity decomposition in a given coordinate system, and leads to approximate governing equations which correct an a priori inviscid solution for viscous effects, secondary flows, total pressure distortion, heat transfer, and internal flow blockage and losses. Solution of the correction equations is accomplished as an initial-value problem in space using an implicit forward-marching technique. The overall solution procedure requires significantly less computational effort than Navier-Stokes algorithms. The present solution procedure is effective even with the extreme local mesh resolution which is necessary to solve near-wall sublayer regions in turbulent flow calculations. Computed solutions for both laminar and turbulent flow compare very favorably with available analytical and experimental results. The overall method appears very promising as an economical procedure for making detailed predictions of viscous primary and secondary flows in highly curved passages.

17. Key Words (Suggested by Author(s))	18. Distribution Statement
Subsonic flow analysis; Secondary flows; Turbulent flow; Curved ducts; Three-dimensional flow computation	Unclassified - unlimited STAR Category 02

19. Security Classif. (of this report)	20. Security Classif. (of this page)	21. No. of Pages	22. Price*
Unclassified	Unclassified	57	A04

* For sale by the National Technical Information Service, Springfield, Virginia 22161

NASA-Langley, 1981